Nanoscale Advances

ROYAL SOCIETY OF CHEMISTRY

REVIEW

View Article Online
View Journal | View Issue

Cite this: *Nanoscale Adv.*, 2025, **7**, 4232

Future development directions of high-temperature strain gauges: a comprehensive review of structure and performance characteristics

Xiang Liu,[a] Zhongkai Zhang,*[a] Jiaxing Wang,[b] Meng Wang,[a] Tao Lin,[b] Yantao Liu,[b] Qing Tan,[c] Rui Qi,[c] Zhaojun Liu*[a] and Bian Tian*[a]

Received 12th January 2025
Accepted 19th May 2025

DOI: 10.1039/d5na00039d

rsc.li/nanoscale-advances

High-temperature strain gauges have garnered significant interest from researchers due to their high precision, exceptional temperature tolerance, and robust anti-interference capabilities. Furthermore, these sensors exhibit a strong linear relationship across a wide range of strain and temperature, making them widely applicable in various fields, including aerospace, the automotive industry, the metallurgical sector, and scientific research. This paper provides a comprehensive review of high-temperature strain gauges, focusing on three main technologies: SAW strain gauges, optical fiber grating strain gauges and TFSGs. We analyze the performance differences among various types of these sensors, systematically summarize several preparation techniques, analyze the performance testing methods for high-temperature gauges, and discuss their current application status and future development directions in related fields.

1. Introduction

Strain sensing materials and technologies have demonstrated extensive applications across diverse fields including solar steam generation,[1] smart textiles,[2,3] microwave absorbers,[4] and bioelectrical signal detection.[5] However, these applications are currently confined to ambient temperature conditions, presenting significant limitations for extreme environment implementation. Advancements in the aerospace and nuclear sectors have necessitated a heightened requirement for the sustained, stable performance of critical components under extreme operational conditions. These components are subjected to high temperatures, high-speed airflow, strong vibrations, high pressures, and rapid temperature changes.[6] To ensure the safety and reliability of these components, accurate and real-time monitoring of their mechanical behavior, particularly strain, is essential. For instance, in the aerospace industry, the ability to monitor strain in jet engines and hypersonic vehicles operating at temperatures exceeding 1000 °C is critical for preventing structural failures and optimizing performance. Similarly, in the nuclear sector, reliable strain measurements are indispensable for maintaining the integrity and efficiency of reactors under extreme thermal and mechanical stresses. The absence of robust high-temperature strain gauges poses significant risks, such as increased likelihood of structural failures, reduced operational efficiency, and higher maintenance costs.

However, traditional strain gauges are limited by the extreme conditions of high temperature, with some sensor components fracturing or failing due to high internal stress.[7] These traditional bonded foil strain gauges have certain drawbacks. The sensitive material is prone to oxidation at high temperatures, limiting its upper working temperature to a maximum of 400 °C,[8] significantly below the requirements for ultra-high temperature testing (exceeding 800 °C). In order to meet the requirements of high temperature measurement, materials with sustained stability above 800 °C are essential. At the same time, an adhesive layer is required to bond foil strain gauges, which increases the loss of strain transmission and leads to greater test errors compared with *in situ* strain gauges. Furthermore, the sensing grid exhibits cross-sensitivity to temperature and strain, where minor temperature fluctuations can induce substantial resistance changes. This phenomenon makes it difficult to distinguish whether the fluctuations in resistance are caused by temperature or strain, thereby increasing the complexity of back-end circuit design and signal processing. Lastly, the installation of traditional strain gauges in high-temperature environments can be complex, necessitating specialized support and protective facilities to ensure proper operation, and thereby requiring highly skilled personnel for installation and maintenance, as the quality of installation directly impacts the accuracy of strain measurement.

Despite the widespread use of conventional strain gauges in various applications, their performance is significantly limited

[a]*State Key Laboratory for Manufacturing Systems Engineering, School of Mechanical Engineering, Xi'an Jiaotong University, Xi'an 710049, China. E-mail: zhangzk@xjtu.edu.cn; lzj2024@xjtu.edu.cn; t.b12@mail.xjtu.edu.cn*

[b]*School of Automation and Information Engineering, Xi'an University of Technology, Xi'an 710048, China*

[c]*Nano & New Materials Research Division, CISDI Research & Development Co., Ltd., Chongqing 401122, China*

under extreme conditions, particularly in high-temperature environments. Issues such as material oxidation, strain transfer errors, and installation difficulties hinder their reliability and accuracy. These limitations not only restrict their applicability in critical industries like aerospace, energy, and automotive engineering but also pose significant safety and efficiency challenges. As industrial processes and technologies increasingly operate under harsh conditions, the demand for robust and accurate strain measurement at high temperatures has become more pressing than ever. This urgency has driven the development of advanced high-temperature strain gauge technologies, which aim to overcome the shortcomings of conventional sensors and provide reliable performance in extreme environments.

High-temperature strain gauges typically utilize surface acoustic wave (SAW) technology, optical fiber grating technology, and resistance strain gauge technology to ensure accuracy and reliability in high-temperature environments. Among the available options, the SAW high-temperature strain gauge boasts attributes including a compact form factor, enhanced sensitivity, and straightforward integration capabilities, rendering it well-suited for the amalgamation of multi-parameter sensing systems. Utilizing the sensing mechanism of SAW, various sensors can be developed to measure additional chemical or physical parameters, including gas, magnetism, and pressure.[9–11] Strain and temperature measurements using optical fiber sensors are predominantly achieved through the utilization of a Fabry–Pérot interferometer (FPI) and fiber bragg grating (FBG).[12] These sensors exhibit stable operation within extreme temperature ranges (typically up to 1000 °C or more), offering high sensitivity and rapid response, thereby meeting the stress and deformation monitoring requirements in diverse high-temperature operating environments. Additionally, sensors based on resistance strain technology can be seamlessly integrated into the surface layer of the component being measured, facilitating direct and accurate deployment.[13] By employing materials with excellent high-temperature stability, such as silicon carbide and silicon nitride, thin film structures are fabricated using micro-electronic processing techniques. The high-precision detection of strain signals is achieved through principles of sensitive resistance, capacitance, piezoelectricity, or electromagnetic induction. Currently, researchers are developing novel materials and structures, such as polymer precursor ceramics (PDCs), which have excellent high-temperature semiconductor properties, piezoresistive effects, and oxidation and corrosion resistance.[14] This paper systematically examines these three types of sensors from the perspectives of their sensing principles and structural designs, providing an in-depth discussion of their material compositions and fabrication processes. Through comprehensive analysis, we elucidate the respective advantages of each sensor type and propose future development directions for high-temperature strain gauges.

2. Principle

The principles underlying high-temperature strain gauges are fundamental to their design and performance. This section provides a detailed analysis of the working mechanisms of these sensors, focusing on their response to strain in extreme environments.

2.1 SAW high-temperature strain gauge

Surface acoustic waves are elastic disturbances that propagate on the surface of solid media, with most of their energy confined to a narrow surface layer near the interface.[15] Sensors that exploit the propagation attributes of SAW are referred to as SAW-based sensors. When subjected to strain, the lattice structure of the piezoelectric material undergoes slight deformation, resulting in changes to its physical properties, such as the elastic constant and density.[16] According to the principles of elastic wave dynamics, the velocity of SAW is influenced by the material's elastic modulus and mass density.[17] Therefore, the application of strain results in alterations to the SAW's propagation velocity. Within a specified strain domain, a direct proportionality is observed between the strain magnitude and the alteration in the SAW's propagation velocity. This linear correlation enables the precise quantification of strain by merely measuring the corresponding changes in the SAW's propagation velocity.

The SAW high-temperature strain gauge primarily relies on Hooke's law and the piezoelectric effect.[18] In accordance with Hooke's principle, the strain that a body undergoes within the confines of elastic deformation is directly proportional to the stress that is imposed upon it. While the SAW high-temperature strain gauge directly measures strain, understanding the relationship between strain and stress is crucial for comprehending the sensor's operation and for converting strain data into stress data if necessary. The formula for Hooke's law is shown in eqn (1).

$$F = kx \tag{1}$$

where F is the force exerted on a body; k is the elastic coefficient of the object, it reflects the ability of the object to resist deformation; and x is the shape variable of the object.

The piezoelectric effect was described by French physicist Jacques Paul. It was first discovered in quartz and tourmaline by Jacques Curie and his brother in 1880.[19] The fundamental tenet of the piezoelectric phenomenon is the application of a pressure force onto a piezoelectric substance.[20] It will produce a potential difference (called the positive piezoelectric effect,[21] Fig. 1a); if a voltage is applied, mechanical stress will be generated (called the inverse piezoelectric effect,[21] Fig. 1b).

2.2 Optical fiber grating high-temperature strain gauge

The optical fiber grating high-temperature strain gauge has found extensive application in structural integrity assessments under extreme thermal and harsh environmental conditions, owing to its compact size, cost-effectiveness, high sensitivity, and strong immunity to electromagnetic interference.[22] An optical fiber grating high-temperature strain gauge is a device that employs fiber grating technology to measure strain under high-temperature conditions.[23] For FBG-based strain gauges,

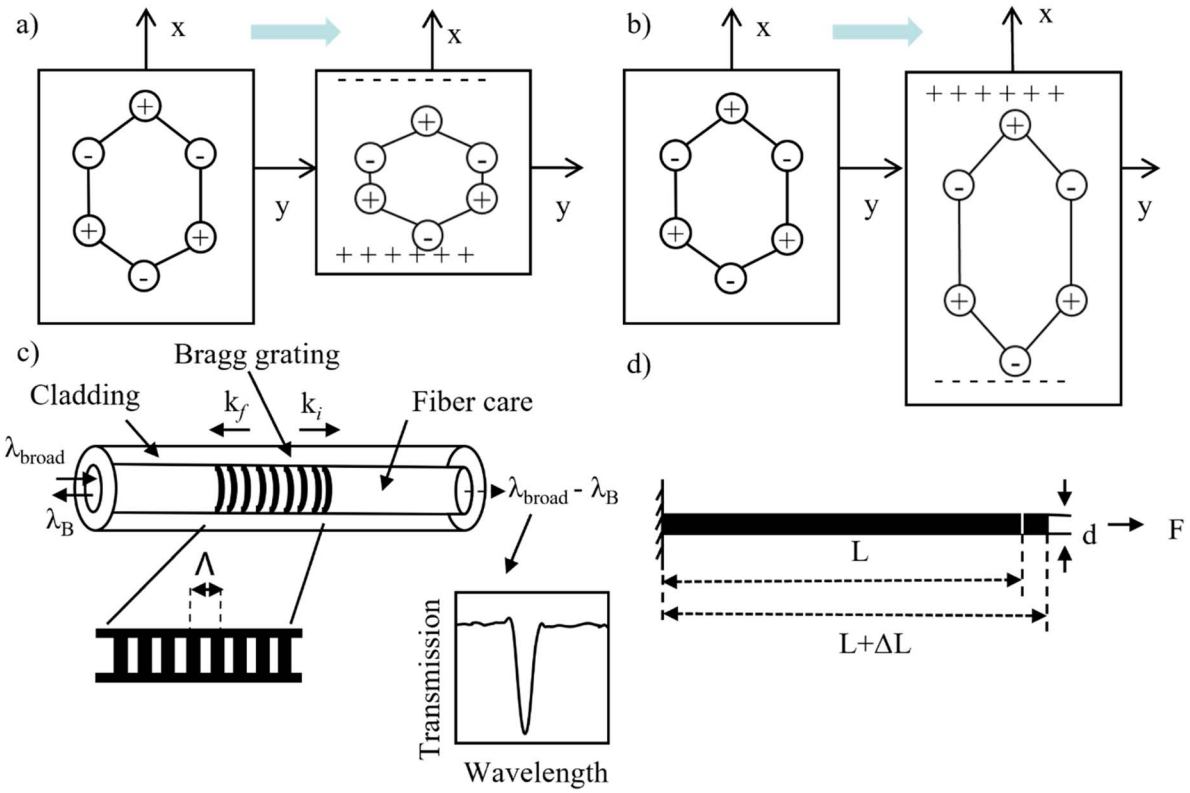

Fig. 1 Schematic diagram of a high-temperature strain gauge: (a) positive piezoelectric effect;[15] (b) negative piezoelectric effect;[15] (c) uniform optical fiber grating structure; (d) schematic diagram of the strain effect of a high-temperature TFSG.

the operational principle relies on the linear relationship between FBG wavelength shift and applied strain, enabling quantitative strain measurement through precise wavelength monitoring. The sensor incorporates a sequence of refractive index fluctuations that are etched into an optical fiber, capable of reflecting particular wavelengths of light. Upon the application of strain to the fiber grating, the grating's periodicity is modified, precipitating a shift in the reflected light's wavelength.[24] By measuring this wavelength variation, the strain experienced by the fiber grating can be accurately assessed. Taking the calculation formula of FBG as an example, the fundamental mathematical expression governing the functionality of an optical fiber grating-based high-temperature strain gauge is presented in the following equation (eqn (2)).

$$\Delta\lambda_b = \lambda_b(1 - P_e)\Delta\varepsilon + \lambda_b(\alpha_f - \varepsilon)\Delta T \quad (2)$$

where λ_b is the initial central reflection wavelength of the fiber grating; $\Delta\lambda_b$ is the change of initial central reflection wavelength; $\Delta\varepsilon$ is the change in strain; P_e is the elastic optical coefficient of the optical fiber; α_f is the thermal expansion coefficient of the optical fiber; ε is the thermo-optical coefficient of the fiber grating; and ΔT is the change in temperature.

For FPI sensors, the relationship between wavelength shift, strain, and temperature change is similar to that of FBG sensors. However, due to the interference-based operating principle of FPI, the response mechanism and formulas differ slightly. Below is the relationship between strain, wavelength shift and temperature change for FPI sensors:

$$\Delta\lambda_b = \lambda_b\Delta\varepsilon + \lambda_b(\alpha_f - \varepsilon)\Delta T \quad (3)$$

Refer to eqn (2) for the description of related symbols.

These formulas illustrate the relationship between the variation in reflected wavelength and the corresponding changes in strain and temperature. In practical applications, when using an optical fiber grating high-temperature strain gauge to measure strain, it is crucial to consider the effects of temperature fluctuations on the wavelength. Therefore, temperature compensation is typically implemented to ensure accurate strain measurement results. Essentially, strain can be calculated using a formula that incorporates the measured wavelength change, known fiber grating parameters, and the temperature variation. Fig. 1c depicts a uniform fiber grating structure.

2.3 High-temperature thin film strain gauge (TFSG)

The high-temperature TFSG serves as a sensing element for measuring strain, relying on the resistance changes induced by mechanical deformation of the component.[25] Under elevated temperature conditions, applied stress induces deformation in the elastic sensitive element, which is subsequently transferred to the resistance strain gauge through both the sensitive element and connecting leads. This deformation generates

a measurable resistance change in the strain gauge, which is then amplified to produce a corresponding electrical signal. However, the inherent thermal instability of thin-film resistance elements under high-temperature operation necessitates the implementation of specialized compensation techniques. In aerospace applications, particularly in advanced aero-engine systems, the increasing demand for performance optimization and intelligent monitoring requires the integration of numerous sensors capable of reliable operation in extreme environments exceeding 1000 °C.[26] When engine blades experience various stresses, they undergo slight deformation; concurrently, the film of the high-temperature strain gauge adhered to the blade surface also generates strain.[27]

TFSG is predominantly realized through the utilization of the piezoresistive mechanism, which is the interplay between the resistive properties of a metallic material and the mechanical strain it experiences.[28] Take the metal material as an example: upon application of a tensile or compressive force (F) to the metallic wire, which is initially characterized by a length (L) and diameter (d), the wire will undergo dimensional alteration, either elongation or contraction. This resultant deformation is directly associated with a corresponding alteration in the wire's intrinsic resistive characteristics (refer to Fig. 1d). Consequently, the derivation of the formula for the high-temperature TFSG is presented below in Formula (4).

$$\varepsilon = \Delta L/L \tag{4}$$

$$\Delta R/R_0 = G_f \cdot \varepsilon \tag{5}$$

where ε is the strain; L is the length of wire; ΔL is the change of length; ΔR is the change in resistance; R_0 is the initial resistance; and G_f is the Gauge Factor (GF).

The SAW high-temperature strain gauge is particularly well-suited for the condition monitoring of metallic structural components within high-temperature, complex environments. It is designed to operate reliably within ambient temperatures as high as 250 °C. An optical fiber grating strain gauge can theoretically be applied to the high temperature strain measurement of structures below 1000 °C, especially for composite structures. Specifically, sensors utilizing a sapphire fiber grating are well-suited for ultra-high temperature measurements exceeding 1800 °C. This is attributed to the sapphire fiber's exceptionally high melting point, approximately 2053 °C, and its minimal transmission loss. The high-temperature TFSG can be engineered as multifunctional integrated sensors capable of simultaneous strain, temperature, and heat flux measurements.

3. Structure

Building on the principles discussed in the previous section, the structural design of high-temperature strain gauges plays a critical role in their functionality and reliability. This section examines the key structural components and configurations that enable these sensors to operate effectively under extreme conditions.

3.1 SAW high-temperature strain gauge

SAW technology incorporates a piezoelectric substrate and an interdigital transducer (IDT). The IDT is engineered to generate a specific pattern on the surface of the piezoelectric substrate. In concert, these elements transform electrical energy into mechanical energy, thereby generating SAW,[29] as illustrated in Fig. 2a. The SAW high-temperature strain gauge primarily comprises a substrate, an electrode, and a protective layer. Typically, piezoelectric materials are employed as the substrate due to their favorable piezoelectric characteristics and high-temperature tolerance. Metal electrodes, such as gold or aluminum, are fabricated on the substrate surface using micro–nano processing technology;[30] these electrodes are essential for generating and detecting SAW. To protect the sensor, it is encapsulated in an external package, generally made from ceramic or other high-temperature materials,[31] ensuring stability in extreme environments. This is often achieved by using a resonator structure, which is a miniaturized MEMS device.[32] The structure primarily involves a combination of an IDT and a reflector (Fig. 2b–d) to form a resonator that can respond to temperature changes and generate frequency variations. An IDT converts electrical signals into SAW through inverse piezoelectric effects. A critical issue in preserving the elevated temperature functionality of SAW sensors revolves around the necessity to improve the thermal robustness of the IDT.[7,33,34]

The function of the reflector is to create a periodic perturbation reflection grid on both sides of the interfingered transducer, enabling the SAW to undergo multiple phase reflections within the resonator.[35] The aforementioned process yields the establishment of a standing wave resonance within the cavity. The development and manufacture of a high-temperature

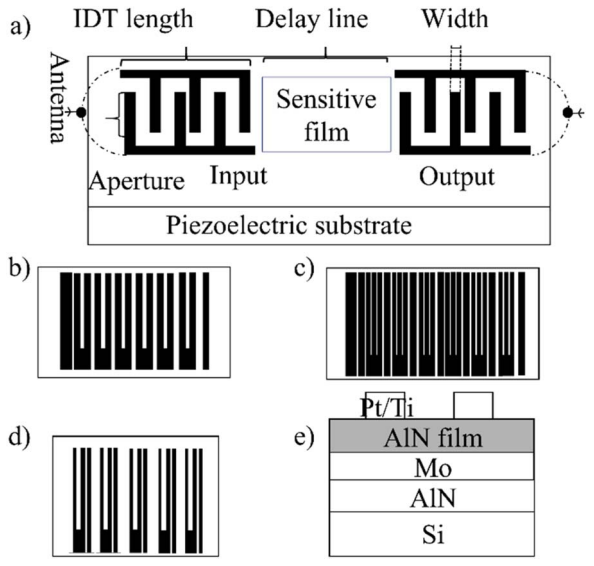

Fig. 2 Structure of SAW high-temperature strain gauges: (a) basic structure;[23] (b) structure diagram of a conventional interdigital electrode;[26] (c) structure diagram of a split interdigital electrode;[26] (d) single phase transducer;[26] (e) structure diagram of a Pt/Ti/AlN/Mo/AlN/Si sensor.[30]

sensor utilizing SAW technology involve a multitude of pivotal considerations, such as the selection of suitable piezoelectric materials, the design of the IDT, the arrangement of the reflector array, the application of a protective coating, and the refinement of the structural design. These components are indispensable for guaranteeing the sensor's superior performance and long-term stability under high-temperature conditions. In 2023, Yong R.[36] successfully developed a high-performance SAW temperature sensor by optimizing the deposition process and structural design. Based on the thermal stability and acoustic properties of various materials, a sensor with a Pt/Ti/AlN/Mo/AlN/Si structure was designed (Fig. 2e), with AlN thin films deposited using reactive radio frequency magnetron sputtering (RF-250W). The particular SAW temperature sensor demonstrated a linear relationship between frequency and temperature, with the frequency–temperature (f–T) curve exhibiting linearity within a temperature spectrum spanning from 20 to 900 °C, achieving a quality factor (Q) of 34.5 and a sensitivity of 46.6 kHz K^{-1}. Through experimental analysis, the performance and application potential of this new SAW temperature sensor in high-temperature environments are demonstrated, alongside potential strategies for further enhancing the sensor's performance.

3.2 Optical fiber grating high-temperature strain gauge

The FBG high-temperature strain gauge predominantly comprises a fiber optic core, an embedded grating structure, and a connecting interface (refer to Fig. 3a). This configuration provides precise detection of minute strain and temperature variations through multiple fiber Bragg gratings (FBGs) inscribed along a single optical fiber, enabling simultaneous multi-point measurements. The sensor's immunity to electromagnetic interference, inherent to its optical fiber composition, ensures reliable operation under complex environmental conditions.

Among the high-temperature strain gauge utilizing FBG, the Mach–Zehnder interferometer (MZI) is the most commonly used to achieve light interference effects (Fig. 3b).[37] A laser

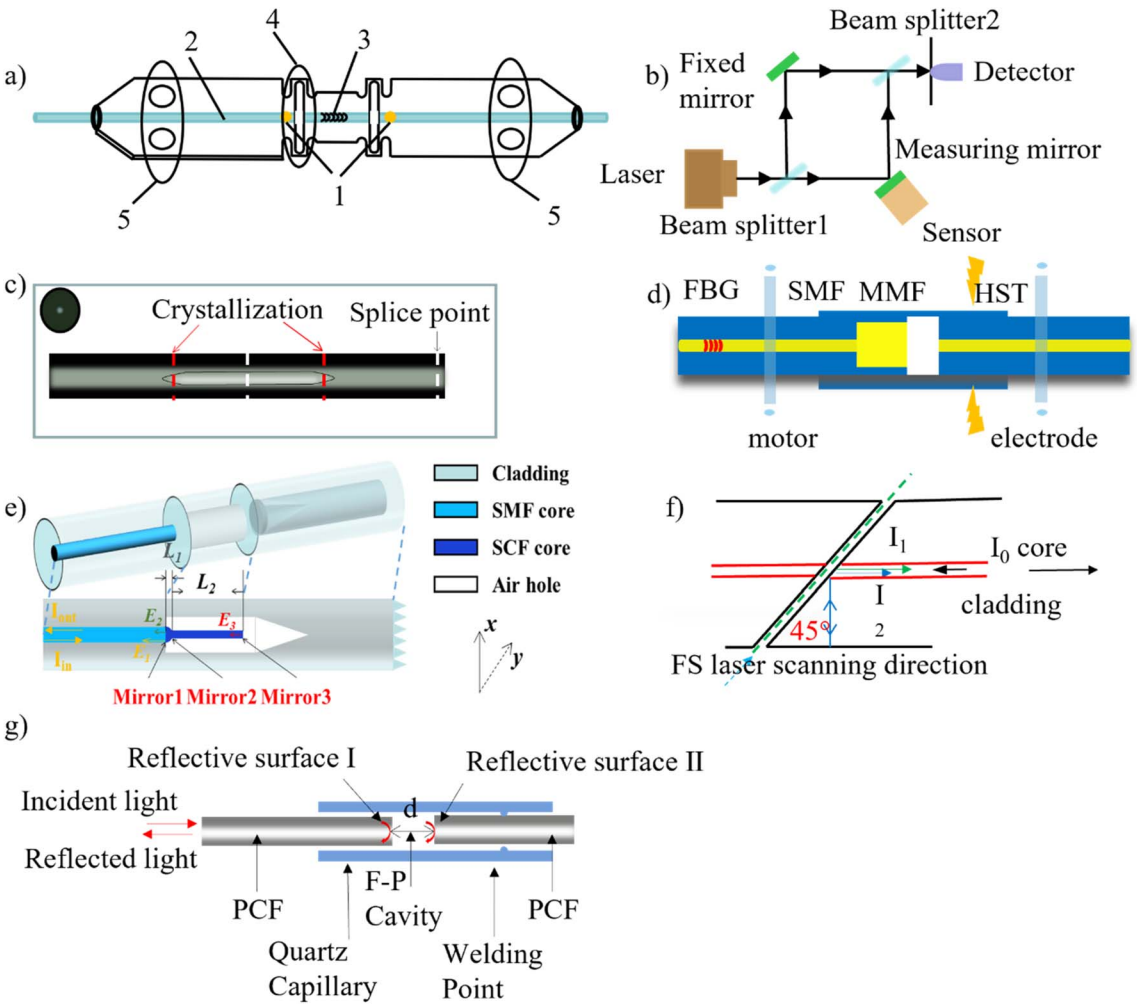

Fig. 3 Structure of the optical fiber grating high-temperature strain gauge: (a) basic structure; (b) schematic diagram of the MZI;[31] (c) schematic diagram of the CDF-FPI sensor;[34] (d) schematic diagram of the FBG-FPI structure;[35] (e) schematic diagram of the sensing structure and working principle based on an FPI;[36] (f) the diagram illustrates the architectural layout of an optical fiber-based sensing probe, with the green dotted line indicating the trajectory of femtosecond laser scanning;[37] (g) schematic diagram of the new PCF F–P sensor.[38]

generates coherent light, which is then channelled into two single-mode fibers of comparable dimensions. One fiber functions as the signal path, while the other acts as the reference path. These two light beams are recombined by a coupler, resulting in an interference effect. The resultant interference can be exploited for the detection of alterations in environmental variables including pressure, thermal conditions, and structural movement.

Additionally, the FPI[38] high-temperature strain gauge represents another significant application. The assembly includes an air-filled cavity and a π-type cavity, which produces a vernier effect due to the superimposition of interference patterns from the air cavity and the air–π hybrid cavity. This effect is instrumental in augmenting the sensitivity of the system for the measurement of relative humidity. Furthermore, the sensor can be combined with an acrylic resin coating and coreless optical fiber, utilizing the material's temperature sensitivity to achieve high-precision temperature measurements.

The FBG high-temperature strain gauge primarily relies on the bragg wavelength shift for strain and temperature measurement. In contrast, fiber-based interferometric gauges, such as the FPI and those utilizing the vernier principle, employ interference phenomena to achieve high-precision measurements. While FBG and interferometric sensors are distinct in their operating principles, they can be complementary in applications requiring both distributed sensing (FBG) and high-resolution point measurements (FPI). The optical interference effect within the sensor is predicated on the superposition principle of light waves, arising from the interaction of light waves traveling through different paths or media.[39] In 2019, as presented by Z. Wang,[40] the ceramic-derived fiber (CDF)-FPI sensor (as depicted in Fig. 3c) was engineered to facilitate accurate strain and temperature measurements through the exploitation of interference phenomena. Z. Wang[40] cut a segment of CDF fabricated using the rod-in-tube technique and spliced both ends with SMF to create a CDF-FPI sensor, which demonstrated high temperature resistance, a broad strain measurement range, and excellent linearity and repeatability. In 2023, Zeren Li[41] integrated a single-mode fiber (SMF) and multimode fiber (MMF) using a commercial welding mechanism to construct an FPI structure (Fig. 3d). In the same year, Siyu Lin[42] introduced a novel high-temperature fiber optic measurement sensor that incorporated a parallel configuration of the F–P interferometer and the Vernier effect (as shown in Fig. 3e), which yielded a remarkable temperature sensitivity of -112.66 pm °C^{-1}.

A 45° fiber optic cantilever beam sensor (Fig. 3f) was manufactured based on the dual-beam interference principle.[43] This sensor exhibited superior consistency and dependability in high-temperature environments, and it was designed to endure temperature extremes up to 1000 °C. Given its diminutive dimensions, cost-effectiveness, and facilitation of large-scale fabrication, the sensor has been engineered for consideration in high-temperature monitoring within restricted areas. In 2020, Ping Xia[44] employed the same fundamental principle to devise an innovative photonic crystal fiber-based Fabry–Pérot interferometric sensor (represented in Fig. 3g). This sensor was capable of measuring mechanical strains as high as 9436.66 με, while maintaining functionality at temperatures as high as 1100 °C. In 2023, Zhongke Zhao[45] leveraged the harmonic vernier effect to attain a temperature-dependent sensitivity of 0.2977 nm °C^{-1}, which notably exceeds that of conventional fiber optic sensors, thereby showcasing superior performance in the domain of extreme temperature measurement. In 2024, Ruyue Shi[46] conducted research into the application of the Vernier effect to amplify the resolution of strain and temperature readings, which was achieved through the integration of the MZI and Sagnac interferometer (SI). The empirical findings revealed a substantial enhancement in the sensor's sensitivity, with the strain measurement sensitivity increasing from 26.7 to -110.92 pm με^{-1}, and the temperature measurement sensitivity improving from -2978 to 7934 pm °C^{-1}.

3.3 High-temperature TFSG

The TFSG is engineered for straightforward deployment within high-temperature operational contexts. The measurement of the material's strain is predominantly achieved through the attachment of a strain gauge featuring a sensitive diaphragm, which translates the mechanical deformation into an electrical output.[47] The operational temperature range of the high-temperature TFSG surpasses 600 °C; at this temperature, the sensor's performance may change significantly, yet it can still maintain a certain level of accuracy. Additionally, the TFSG boasts enhancements including superior temperature constancy, a negligible temperature-dependent coefficient, and robust dependability, positioning it as a favourable candidate for use in environments subject to extreme temperatures.

The fundamental configuration of a high-temperature strain gauge employs a strain-responsive grid, electrical contacts, a supporting substrate, conductive pathways, and a protective overlay.[48–50] The strain-sensitive grid serves as the core component, consisting of several grid bars designed to sense external stress or strain. The geometry, size, and material of the sensitive grid directly influence its response to strain. By optimizing these factors, the sensor can detect smaller strain changes, enhancing its sensitivity, stability, and reliability. The electrodes within the high-temperature TFSG are situated at the extremities of the strain-sensitive element and are generally crafted from a metallic foil or conductive polymer, facilitating the conversion of the strain signal into an electrical signal. The supporting substrate, located beneath the sensitive layer, provides mechanical support and is often constructed from high-strength, high-temperature-resistant materials such as Al_2O_3 and SiO_2.[49–51] The leads connect the electrodes to the external circuit and may be made of metal wire or conductive polymer wire. Adhesives are employed to secure the electrodes and leads, ensuring they remain intact in external environments; common materials include high-temperature adhesives, silver paste, and platinum paste. The protective layer encases the entire strain gauge to shield it from harsh environments and chemical corrosion. The protective coating must demonstrate resistance to oxidative degradation and thermal stability, with its thermal expansion coefficient being substantially

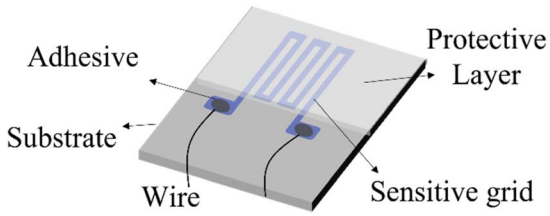

Fig. 4 Basic structure of the TFSG.

similar to that of the sensitive layer to avert delamination at elevated thermal conditions. The detailed design and the corresponding fabrication methods are depicted in Fig. 4.

The SAW high-temperature strain gauge, optical fiber grating high-temperature strain gauge and high-temperature TFSG are three kinds of sensors to monitor strain in high temperature environments, and each of them has unique structural characteristics. Among them, the SAW sensor structure includes an IDT and a reflection gate, which work together to improve sensitivity and selectivity. The structure of an optical fiber grating high temperature strain gauge includes the grating itself as well as possible packaging techniques to protect the grating from environmental influences. The high-temperature TFSG incorporates the application of thin-film processing to sequentially deposit a multitude of layers onto the supporting base. These layers encompass a strain-responsive element, an isolating layer, a layer with functional properties, and a layer designed for protective purposes. Their structural design needs to consider thermal expansion, spalling and diffusion problems, as well as stability at high temperatures. Each of the three sensors is adapted to different application scenarios, and their structural characteristics allow them to provide reliable strain measurement in high-temperature environments.

4. Materials and fabrication

4.1 SAW high-temperature strain gauge

Compared with a conventional high-temperature metallic strain gauge, the SAW high-temperature strain gauge is gaining prominence. These sensors are employed to monitor strain, as well as additional parameters such as temperature and pressure. Their adoption is attributed to their superior sensitivity and robust temperature stability characteristics.[52] However, the stability and performance of materials employed in conventional SAW sensors often face limitations at elevated temperatures. This challenge has prompted researchers to investigate new materials and structures to enhance sensor performance. Common substrate materials for the traditional SAW high-temperature strain gauge include lead zirconate (PZT)[53] and lithium niobate ($LiNbO_3$),[54] which serve to support the sensor and facilitate sound wave propagation. Typically, thin film platinum is used to deposit metal electrodes, arranged in a specific configuration to generate SAW. The sensor measures strain by utilizing phase changes in surface waves as sound waves propagate through an area configured with electrodes. Although traditional SAW sensors can operate in high-temperature environments, the thermal resistance of the substrate materials and electrodes remains limited. Additionally, the relatively large size of conventional structures restricts the application of the SAW high-temperature strain gauge in confined spaces. Table 1 provides a detailed investigation of some common parameters in the SAW high-temperature strain gauge. By analyzing the parameters in each column of the table, the advantages and limitations of each design can be identified, providing valuable insights for the development of this sensor.

The development of high-temperature strain gauges necessitates a careful balance among material selection, fabrication techniques, and temperature decoupling methods, each of which plays a critical role in determining sensor performance. Among piezoelectric materials, LGS and AlN (002) are particularly promising for high-temperature applications due to their exceptional thermal stability and adaptability. LGS, with its outstanding temperature tolerance (up to 800 °C) and versatility in crystal orientations, is well-suited for extreme environments. For example, when integrated with Pt–Rh/Al_2O_3 electrodes, LGS sensors exhibit remarkable thermal stability and oxidation resistance, making them ideal for demanding applications such as aerospace and energy systems. Similarly, AlN (002) offers excellent thermal stability (up to 550 °C) and is compatible with magnetron sputtering, a precise fabrication method that ensures high-quality thin films. These materials, combined with advanced temperature decoupling techniques such as the dual-channel SAW sensor design, enable accurate strain measurements even under harsh conditions.

In contrast, materials like $LiNbO_3$ and *Y*-cut 35° *X* quartz, while providing high GF, are limited by their lower maximum operating temperatures (250 °C and 80 °C, respectively). For instance, $LiNbO_3$ demonstrates a GF of 100 Hz $\mu\varepsilon^{-1}$ and is fabricated using photolithography and ion beam etching, but its inability to withstand extreme temperatures restricts its use in high-temperature environments. Similarly, quartz-based sensors, despite their high sensitivity (598 Hz $\mu\varepsilon^{-1}$) and self-temperature compensation capabilities, are confined to low-temperature applications due to their limited thermal stability. These limitations underscore the inherent trade-off between sensitivity and temperature tolerance, which must be carefully evaluated based on the intended application.

The selection of interdigital electrode materials further significantly influences sensor performance. For high-temperature applications, Pt–Rh/Al_2O_3 and Pt–Ni|Pt–Zr electrodes are particularly effective due to their exceptional thermal stability and oxidation resistance. However, these materials often require complex fabrication techniques, such as atomic layer deposition (ALD), which increase production costs and complexity.

In conclusion, the development of a high-temperature strain gauge requires a strategic balance among material properties, fabrication techniques, and temperature decoupling methods. While materials like LGS and AlN, combined with advanced electrodes and fabrication technologies, offer superior performance for extreme environments, their complexity and cost must be weighed against simpler, more cost-effective alternatives such as $LiNbO_3$ and quartz-based sensors. This analysis

Table 1 Comparison of materials and performance of the SAW strain gauges investigated

Piezoelectric material	Interdigital electrode material	Gauge factor (GF)	Temperature decoupling method	Maximum temperature	Preparation technology	Reference
$LiNbO_3$	Cr/Pt (20/180 nm)	100 Hz $\mu\varepsilon^{-1}$	Dual-channel SAW sensor design	250 °C	Standard photolithography and ion beam etching	X. Li[9]
Langasite (LGS)	Ti/Pt (10/160 nm)	63 Hz $\mu\varepsilon^{-1}$	Frequency domain decoupling	500 °C	Standard photolithography and lift-off process	Jikai Zhang[52]
LGS	Pt–Rh/Al_2O_3	Nonlinear	—	800 °C	Standard photolithography and lift-off process	Jikai Zhang[55]
AlN (002)	Ti/Pt (10/100 nm)	0.84 ppm $\mu\varepsilon^{-1}$	Dual-channel SAW sensor design	550 °C	Magnetron sputtering system	Fanbing Hu[56]
LGS (0, 138.5°, 26.7°)	Pt–Ni|Pt–Zr (15 nm eachwith 5 layer)	−41 Hz $\mu\varepsilon^{-1}$	Dual-channel SAW sensor design	400 °C	Atomic layer deposition (ALD)	Anin Maskay[57]
Y-Cut 35° *X* quartz	Al (120 nm)	598 Hz $\mu\varepsilon^{-1}$	Self-temperature compensation	80 °C	Standard photolithographic technique	Wen Wang[58]
c-Axis AlN	Ti/Au (10/110 nm)	303.12 Hz $\mu\varepsilon^{-1}$	—	400 °C	Standard photolithography techniques	L. Shu[59]
LGS (0, 138.5°, 117°)	Ti/Au (10/100 nm)	350 Hz $\mu\varepsilon^{-1}$	Compensating film techniques	500 °C	Standard photolithography techniques	Shu Lin[60]

highlights the importance of tailoring sensor design to specific application requirements, ensuring optimal performance under high-temperature conditions.

The structure of the SAW high-temperature strain gauge has been enhanced through the utilization of novel substrates and electrode materials in recent years. For instance, materials such as monocrystalline silicon and aluminum nitride (AlN)[61,62] have been employed, resulting in ALN-based SAW resonators that not only exhibit superior performance but also demonstrate compatibility with CMOS technology compared to other piezoelectric devices.[63] In 2020, Jeremy Streque[64] adopted an aluminum nitride/sapphire structure, using aluminum as the electrode material (Fig. 5a). The low density and resistivity of the aluminum electrode significantly reduce mechanical losses and enhance the quality factor (Q value),making this sensor a viable alternative to traditional heavy metal electrodes, such as platinum, for high-temperature wireless sensing. In 2022, Xiawen Yan[65] introduced another high-temperature stable substrate, further extending the potential applications of SAW sensors under extreme conditions. In particular, a SAW high-temperature strain gauge was developed using LGS as the base material, with the (0°, 138.5°, 117°) direction serving as the tangential orientation for the LGS substrate in the sensor's fabrication (refer to Fig. 5b and c). At a temperature of 700 °C, the sensor exhibits a GF of 20.09 Hz $\mu\varepsilon^{-1}$, accompanied by a maximum relative error of 3.35% and a hysteresis error of 6.98%. This performance underscores a notable improvement in the sensor's dependability and precision under high-temperature conditions, offering a richer dataset compared to earlier research findings. The incorporation of new substrate and electrode materials allows SAW sensors to be utilized in extremely high-temperature environments. Furthermore, the application of advanced micro- and nano-manufacturing technologies facilitates the development of smaller sensors, making them suitable for more complex application environments. The transition from traditional substrate materials and larger sizes to innovative materials and micro-structures has markedly improved the sensitivity and adaptability of the SAW high-temperature strain gauge.

The advancement of wireless technology has enabled the integration of SAW sensors with wireless communication, facilitating remote monitoring and data transmission. This capability is especially valuable in specific environments. By selecting appropriate piezoelectric materials and optimizing the structural design of the device, sensors can achieve high sensitivity[66] and a high Q value. Additionally, by choosing the tangent direction of the characteristic axis of the anisotropic piezoelectric crystal, it is possible to mitigate the temperature interference on the SAW sensor, thereby achieving effective temperature compensation. Advancements in the field of high-temperature strain gauge leveraging SAW technology are being realized across the domains of materials science, operational capabilities, practical applications, and technological refinement. These developments suggest considerable potential for utilization and market viability. As scientific research and technological advancements continue to evolve, this field is poised for further growth in the future.

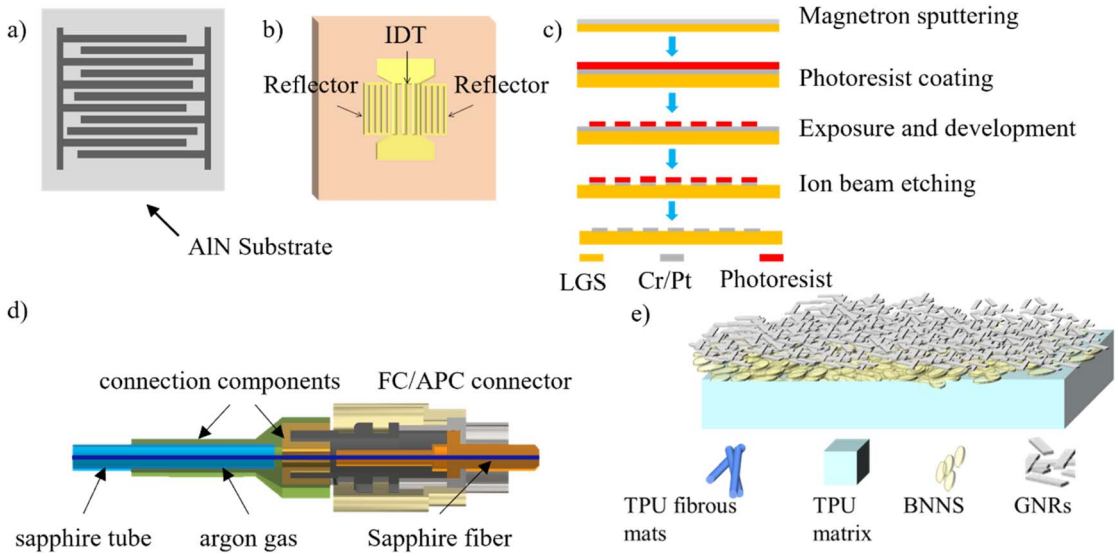

Fig. 5 Material and fabrication diagram of the SAW high-temperature strain gauge and optical fiber grating high-temperature strain gauge: (a) ALN substrate low frequency SAW device;[52] (b) resonant SAW sensor based on Langa stone;[53] (c) preparation process of the resonant SAW sensor based on Langa stone;[53] (d) schematic diagram of an ultra-high temperature sensor;[58] (e) wearable strain gauge based on a thermoplastic polyurethane (TPU) substrate.[59]

4.2 Optical fiber grating high-temperature strain gauge

Traditional FBG high-temperature strain gauges often face limitations due to the failure of conventional optical fiber grating materials at extremely high temperatures.[67] Additionally, the optical fiber exhibits a degree of fragility and is prone to externally-induced degradation, thereby undermining the integrity and dependability of the sensor. To address these challenges, researchers have enhanced the sensor's structure by applying a protective coating to the exterior of the fiber, thereby improving its tensile and impact resistance. Furthermore, the use of high-temperature resistant fiber materials, such as fluoride fiber or ceramic fiber, significantly enhances the sensor's thermal resilience.[68,69] The transition from a traditional optical fiber to advanced high-temperature fiber, coupled with a reinforced protective layer, has led to substantial improvements in the temperature resistance, sensitivity, and mechanical strength of the optical fiber grating high-temperature strain gauge.

To enhance stability and oxidation resistance at extreme temperatures, new fiber materials, such as sapphire fiber and photonic crystal fiber (PCF), are increasingly utilized. In 2022, Jia He[70] proposed an ultra-high temperature sensor utilizing femtosecond laser writing and an inert gas sealing package (Fig. 5d). This designed sapphire FBG sensor capitalizes on the high melting point of sapphire fiber, enabling continuous operation for 20 hours at a high temperature of 1600 °C. Through third-order polynomial fitting, the repeatability of this ultra-high temperature sensor is improved, achieving a temperature sensitivity of 41.9 pm $°C^{-1}$ at 1800 °C. The sensor mitigates the limitations inherent to conventional sensors under ultra-high temperature conditions, such as high-temperature oxidation and performance degradation, making it suitable for extreme temperature monitoring in the aviation and power industries. This demonstrates its practical potential in strain sensing applications. In the same year, Cenxiao Tan[71] developed a high-performance wearable strain gauge (Fig. 5-e),employing thermoplastic polyurethane (TPU) as the base material. Graphite nanoribbons (GNRs) were deposited onto an electrospun TPU fiber film using vacuum filtration deposition technology to create a conductive network. Additionally, the thermal conductivity of the TPU was enhanced by incorporating boron nitride nanosheets into the TPU matrix. Experimental results indicate that the sensor exhibits stable thermal performance and a highly sensitive strain response across a strain range of 0 to 100%. This development provides a wearable strain gauge that combines excellent mechanical properties with advanced thermal management capabilities, thereby opening new possibilities for wearable device innovation, particularly in scenarios subject to extreme thermal stress, and highlighting the potential of these sensors in practical applications such as monitoring human joint movement.

FPI sensors provide an alternative approach with higher precision for point measurements. The materials used in FPI sensors are similar to those of FBG sensors. However, the fabrication of FPI sensors requires the creation of a resonant cavity between two reflective surfaces, which can be accomplished through several advanced techniques, each with its own advantages and limitations. Fusion splicing,[72] which involves fusing two optical fibers with a small air gap to form an intrinsic FPI cavity, is a simple and cost-effective method suitable for large-scale production; however, it suffers from limited precision in controlling the air gap length and reduced mechanical strength at high temperatures. In contrast, laser micromachining,[73] utilizing ultrafast lasers to create micro-cavities directly within the fiber, offers exceptional precision and flexibility, making it ideal for high-performance applications,

Table 2 Comparison of materials and performance of the optical fiber grating high-temperature strain gauges investigated

Sensing structures	Gauge factor (GF)	Temperature decoupling method	Maximum temperature	Preparation technology	Reference
2 FBG	0.312 dBm $\mu\varepsilon^{-1}$	Mathematical model compensation	100 °C	—	Chiranjit Ghosh[74]
A type II fine-core pure silica FBG with a type I Ge-doped regenerative FBG	1.5 pm $\mu\varepsilon^{-1}$	Dual-grating method	550 °C	A tapered splicing technique and femtosecond laser technology	Chen Wang[75]
Type II FBG and a miniature fiber FPI	1.74 pm $\mu\varepsilon^{-1}$	—	600 °C	Fusion splicing and femtosecond laser pulses	Yajun Jiang[76]
A FPI based on an alumina CDF	1.5pm $\mu\varepsilon^{-1}$	—	1000 °C	Rod-in-tube technique and fusion splicing	Zhi Wang[40]
A parallel dual fiber FPI	178.75 pm $\mu\varepsilon^{-1}$	Dual-grating method	900 °C	Fusion splicing and femtosecond laser technology	Zeren Li[41]
An ultrasensitive parallel double FPI sensor based on the vernier effect and type II FBG	127.32 pm $\mu\varepsilon^{-1}$	Temperature compensation grating	1000 °C	Fusion splicing and femtosecond laser pulses	Xin Liu[77]
A silica-cavity intrinsic FPI cascading an air-cavity extrinsic FPI	0.0145 μm $\mu\varepsilon^{-1}$	Temperature compensation grating	1000 °C	Fusion splicing	Ping Xia[44]
An extrinsic FPI with unlimited cavity length and a gold-coated regenerative FBG	21.46 nm $\mu\varepsilon^{-1}$	Temperature compensation grating	800 °C	Fusion splicing	Jian Nan[78]
A cascaded fiber FPI-regenerated FBG	2.17 pm $\mu\varepsilon^{-1}$	Temperature compensation grating	1000 °C	Fusion splicing	Qin Tian[79]

although the high cost of equipment and complexity of the process pose significant challenges. The CDF-FPI sensor fabricated by Z. Wang[40] using fusion splicing demonstrated a GF of 1.5 pm $\mu\varepsilon^{-1}$ at 900 °C, maintaining a linear response over a strain range of 0 to 3000 με. Furthermore, the sensor is capable of operating at temperatures up to 1200 °C, achieving a temperature sensitivity of 15.6 pm $°C^{-1}$ at its maximum operating temperature, as depicted in Fig. 3c. By leveraging the principles of interference, the GF of the sensor made by Zeren Li[41] was significantly improved to 178.75 pm $\mu\varepsilon^{-1}$ *via* the application of the fiber Vernier harmonic effect. The sensor demonstrated an excellent linear response to both strain and temperature changes across the operational range of 24 to 900 °C. Table 2 provides a comprehensive comparison of various sensing structures used in high-temperature strain gauges, highlighting their GF, temperature decoupling methods, and fabrication techniques. By analyzing these parameters, we can evaluate the strengths and limitations of each design, offering insights into their suitability for specific high-temperature applications.

By analyzing this table, it can be concluded that FPI-based sensors, such as the alumina CDF FPI and the ultrasensitive parallel double FPI, stand out for their exceptional temperature tolerance (up to 1000 °C) and high GF (*e.g.*, 127.32 pm $\mu\varepsilon^{-1}$ for the Vernier-effect FPI). These sensors leverage advanced fabrication techniques like femtosecond laser technology and fusion splicing, making them ideal for extreme environments. In contrast, FBG-based sensors, like the Type II FBG with RFBG, offer moderate GF (1.5 pm $\mu\varepsilon^{-1}$) and lower temperature tolerance (550 °C), limiting their use to less demanding applications. Hybrid structures, such as the cascaded IFPI-EFPI, combine the benefits of both FPI and FBG designs, achieving high temperature tolerance (1000 °C) and reliable performance. Temperature decoupling methods, such as dual-grating techniques and temperature compensation gratings, are critical for ensuring accurate measurements in high-temperature environments. While FPI-based sensors often incorporate these methods effectively, FBG-based sensors rely on simpler approaches like mathematical model compensation, which may not be as robust under extreme conditions.

In conclusion, FPI-based sensors are superior for high-temperature applications due to their higher temperature tolerance and GF, while FBG-based sensors are better suited for moderate-temperature environments. The choice of sensor design should align with the specific requirements of the application, balancing performance, complexity, and cost. The high-temperature strain gauge based on optical fibers has been continuously developed in terms of material, performance, application, and technical advancements, demonstrating promising potential for various applications. As technology progresses, its use in structural monitoring, industrial applications, aerospace, and other fields is expected to expand significantly.

4.3 High-temperature TFSG

The selection of materials and the application of manufacturing techniques are decisive factors in determining the efficacy of

high-temperature TFSGs. When selecting experimental materials, thin-film substances with high-temperature stability and excellent electrical properties, such as indium tin oxide (ITO),[80] tungsten, or platinum, are typically employed, as they maintain stable resistance and sensitivity in extreme environments. In the manufacturing process, magnetron sputtering technology is commonly utilized for thin film deposition, ensuring the uniformity and adhesion of the material layer. Furthermore, advancements in inkjet printing technology have enabled the production of high-precision thin film patterns, thereby enhancing the measurement accuracy and reliability of the sensors. These advanced materials and manufacturing techniques allow high-temperature strain gauges to accurately monitor strain under harsh conditions, fulfilling the demand for high-performance sensors in aerospace, energy, and other fields.

Research on high-temperature strain gauges based on resistance strain gauges began earlier in foreign countries. During the 1960s, the United States' NASA initiated a series of research endeavors focused on a range of thin-film sensors, which were specifically engineered for the surface-based monitoring of aerospace engine turbine blades.[47,81] The high-temperature TFSG emerged as a significant component of this research. With ongoing exploration by subsequent researchers, a series of notable findings have been achieved. In recent years, advancements in high-temperature strain gauges utilizing resistance strain gauges have been particularly impressive, especially concerning material selection and manufacturing processes. In 2019, Hao Liu[82] successfully prepared a PdCr strain gauge on a nickel-based superalloy (K465) test strip using vacuum sputtering deposition technology (Fig. 6a). They examined the linear change characteristics of the PdCr TFSG in response to both static and dynamic strains at elevated temperatures. The findings suggest that the strain gauge exhibits superior repeatability and dependability in high-temperature environments, thereby justifying a more in-depth investigation into the material's characteristics under such thermal conditions. In the same year, Shenyong Yang[83] developed an indium tin oxide (ITO) ceramic strain using a magnetron sputtering process (refer to Fig. 6b) and examined the impact of air and nitrogen (N_2) thermal treatments on the piezoresistive response of the ITO ceramic strain gauge at 1200 °C, along with the morphology of the ITO ceramic strain gauge featuring Pt contact pads (refer to Fig. 6c). The research outcomes disclose that the nitrogen-treated ITO ceramic strain gauge presents a reduced yet more consistent GF at elevated

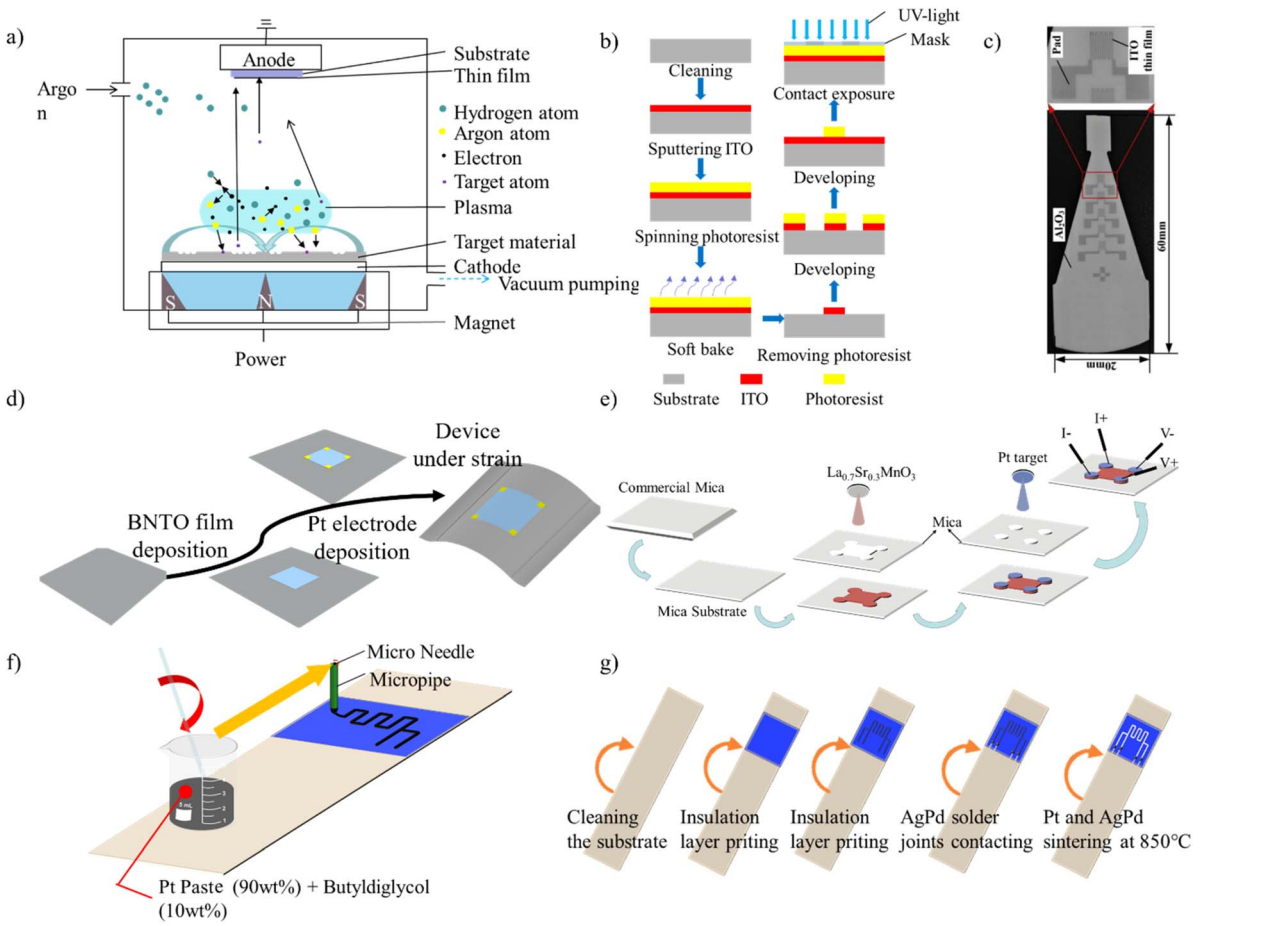

Fig. 6 Material and fabrication diagram of high-temperature TFSGs: (a) schematic diagram of vacuum sputtering deposition technology;[62] (b) morphology of an ITO ceramic strain gauge with a Pt pad deposited on an Al_2O_3 substrate;[63] (c) TFSG process of ITO;[65] (d) ITO optical images with a Pt pad;[65] (e) preparation of LSMO film;[66] (f) Pt slurry DIW process diagram;[68] (g) process flow chart of a Pt film strain gauge.[69]

temperatures, underscoring the significant effect of nitrogen-based heat treatment on the piezoresistive characteristics of the material. However, it was also observed that the piezoresistive characteristics of the sensor remain unstable at high temperatures following nitrogen heat treatment. In 2022, Zhichun Liu[84] aimed to optimize the nitrogen partial pressure of ITO films to enhance their piezoresistivity stability at elevated temperatures, employing the TFSG process during preparation. At 600 °C, an increase in nitrogen partial pressure resulted in a decrease in the gauge factor (GF) of the strain gauge from 2.28 to 1.48, attributed to a reduction in the quantity of electron ionization. Conversely, at 800 °C and 1000 °C, an ITO film strain gauge with a nitrogen partial pressure of 20% exhibited the highest GF. By optimizing the nitrogen partial pressure, the piezoresistive stability and response of the ITO thin-film strain gauge at high temperatures can be significantly enhanced, thus contributing to a deeper understanding of high-temperature strain measurement.

In terms of material selection, several studies have highlighted the advantages of new materials and their composite structures. In 2019, Cheng Yang[85] demonstrated exceptional sensitivity at extreme temperatures (GF = 27.5) by employing pulsed laser deposition (PLD) to deposit BNTO films on a mica substrate (Fig. 6d). The selection of materials and the structural configuration facilitate consistent functionality over an extensive temperature spectrum from 20 to 773.15, representing a significant improvement over traditional flexible strain gauges. In 2020, Min Guo[86] designed a flexible strain gauge that incorporated a functional oxide, $La_{0.7}Sr_{0.3}MnO_3$ (LSMO), onto a mica support, employing the pulsed laser deposition technique once more (refer to Fig. 6e) The LSMO/mica strain gauge exhibits good sensitivity, with a resistance change rate of 5.0% at a bending radius of 3 mm. Upon completion of 3600 bending cycles followed by release, the device exhibited a resistance change rate that was less than 0.5%, which underscores its superior endurance. The remarkably high resistance variation ratio and durability under bending conditions further highlight the potential applications of functional oxide materials in high-temperature flexible sensors. In 2021, Yilong Li[87] conducted research on an inorganic-based flexible high-temperature strain gauge that employed a $SrRuO_3$ (SRO) film integrated with a mica heteroepitaxial architecture. The developed thin-film sensor exhibited a substantial resistance variability of 26.05% under ambient conditions, along with a notable GF of 101, which attests to its high linearity.

During the investigation into high-temperature TFSGs that are based on resistance strain gauges, an innovative fabrication technique has been developed to mitigate the drawbacks associated with established manufacturing processes. In 2022, Chao Wu[88] introduced direct ink writing technology (DIW), which provides a novel preparation approach for a silver–palladium TFSG (Fig. 6f and g). This method demonstrates excellent static and dynamic responses, particularly at high temperatures, without significant attenuation. Additionally, the research team utilized an Al_2O_3-functionalized polymer-derived ceramic silicon nitride (SiCN) coating to augment the robustness and operational longevity of the sensor under harsh conditions. This suggests that the sensor's overall performance has been significantly elevated as a result of advancements in protective coating technology. High-temperature strain gauges based on resistance strain gauges are rapidly evolving, and their potential applications and market demand are expected to grow alongside advancements in materials science and manufacturing processes. Advancements in the materials and structural design of high-temperature TFSGs have markedly improved their functional efficacy under severe environmental conditions, thereby enhancing measurement precision and broadening their potential applications. This new design concept and material selection represents a significant advancement in sensor technology, laying a solid foundation for future applications.

Among them, the high-temperature strain gauge made of metal materials has significant potential demand in aerospace, petroleum exploration, industrial smelting, and other fields. This is due to the inherent limitations of conventional electrical sensors, which are unable to sustain precise measurements over extended durations in adverse environments characterized by high temperatures, elevated pressures, intense electromagnetic disturbances, and chemical erosion.[89,90] To address these challenges, the research team developed several types of high-temperature strain gauges. The strain gauge designed for high-temperature operation, which incorporates semiconductor components, detects strain by capitalizing on the intrinsic alteration in resistivity of semiconductor materials as they are subjected to mechanical stress. This type of sensor exhibits high sensitivity and good temperature stability. Current research and applications indicate that the semiconductor strain gauge primarily leverages the piezoelectric effect of semiconductor materials such as silicon and germanium to detect pressure or strain by measuring changes in resistivity.[91,92] These sensors are often designed to maintain high nominal resistance under both positive and negative strain, rendering them more sensitive than metal film sensors in certain situations. Despite this, the semiconductor strain gauge exhibits a pronounced sensitivity to temperature variations, and the correlation between resistance alterations and applied strain is often non-linear, introducing complexities when these devices are utilized in high-temperature contexts.

Moreover, most TFSG's performance is considerably affected by temperature variations, necessitating accurate temperature compensation. The temperature compensation of the strain gauge generally involves the following methods: self-compensation, bridge compensation, software compensation, and dual-grid compensation. Among these, the self-compensation strain gauge typically achieves self-compensation within a specific temperature range by selecting appropriate sensitive grid materials and substrate materials to match the thermal output (resistance changes due to temperature) of the strain gauge with the thermal expansion coefficient of the material being tested. However, this method is only applicable in scenarios where the thermal expansion coefficient of the material being tested is known. Bridge compensation involves the use of one or more dummy gauges in a Wheatstone bridge. These compensation strain gauges,

placed in the same temperature environment as the working strain gauge but not subjected to strain, offset the resistance changes caused by temperature through the differential characteristics of the bridge. Software compensation, also known as the tabular method, establishes the relationship between temperature and strain gauge output through experiments or theoretical models. Algorithms are then utilized to provide real-time corrections to the measurement data. This method requires precise temperature sensors and sophisticated data processing capabilities. Dual-grid compensation involves fabricating two sensitive grids in the strain gauge with identical materials and structures. One grid is used to measure strain, while the other is used to measure temperature changes. The difference in output between the two grids is used to eliminate the effects of temperature. However, the compensation accuracy of this method is limited by the fabrication precision. Currently, most researchers employ self-compensating methods to mitigate the temperature effects on strain gauges. Differing from the aforementioned approach, researchers combine two sensitive materials with opposite TCR values and develop TFSGs with TCR approaching 0 through stacking or mixing techniques to achieve temperature compensation. For instance, Chao Wu[93] combined graphite nanoplates (GNPs) with positive TCR and polysilazane (PSN2) with negative TCR in varying proportions, printing a TFSG using DIW. This yielded a strain gauge with an approximate TCR of 3.7 ppm $°C^{-1}$ between 30 and 300 °C.

It is pertinent to note that the calibration of TFSGs is commonly performed under high-temperature conditions, involving the tensile deformation of the gauge. The sensor's performance characteristics are quantified through comparative evaluation against reference strain gauges under identical loading conditions, or alternatively, *via* theoretical modeling of the resistance-strain relationship during tensile deformation. To facilitate a comparative analysis of the impact of diverse materials and fabrication techniques on the performance of TFSGs, we have, based on a synthesis of the pertinent literature, compiled Table 3, which outlines the various performance indicators of interest for TFSGs, including the GF, the temperature coefficient of resistance (TCR), and the upper operational temperature limit, for reference.

From the summarized table, it is evident that only a small fraction of researchers have considered high-temperature alloy substrates in their selection. While this approach may simplify the preparation of the insulating layer for strain gauges, it offers limited reference value for the engineering application of these gauges. For instance, aerospace turbine blades and high-temperature metallurgical furnace shells are typically fabricated from high-temperature alloys. Strain testing on such

Table 3 Comparison of the materials and performance of various strain gauges investigated

Base material	Sensitive layer material	Gauge factor (GF)	TCR	Maximum temperature	Preparation technology	Reference
Al_2O_3	Graphene	—	0.29%/°C	600 °C	Magnetron sputtering technology	Chenggang Tang[94]
GH3536	Pt	1.94 (25 °C) 1.9 (600 °C) 1.7 (700 °C)	—	700 °C	DIW	Xiaochuan Pan[95]
Al_2O_3	TiB_2/SiCN	4.28	1.6 ppm $°C^{-1}$	700 °C	DIW	Chao Wu[96]
Al_2O_3	AgPd	1.25 (25 °C) 1.2 (600 °C)	638 ppm $°C^{-1}$	800 °C	DIW	Chao Wu[97]
Al_2O_3	ITO	15 (N_2-ITO, 1200 °C)	−778 ppm $°C^{-1}$ (N_2-ITO) 797 ppm $°C^{-1}$ (air-ITO)	1200 °C	Rf magnetron sputtering technology	Shenyong Yang[83]
High purity Al_2O_3	ITO	2.28 (600 °C 2.66 (800 °C)	—	1000 °C	Rf magnetron sputtering technology	Zhichun Liu[98]
99% Al_2O_3	ITO	8.12 (800 °C)	−521 ppm $°C^{-1}$	1100 °C	Pulsed laser deposition technology	Shuolin Li[7]
GH3536	Pt	2.55 (30 °C) 1.09 (800 °C)	1730 ppm $°C^{-1}$	800 °C	DIW	Chao Wu[88]
96 wt% Al_2O_3	ITON	1.8–2.1 (N_2–air, 1000 °C)	1047 ppm $°C^{-1}$	1200 °C	Rf magnetron sputtering technology	Zhichun Liu[84]
GH3536	TiB_2/SiCN	7.12 (T60, 25 °C 4.12 (T70, 70 °C)	−386 ppm $°C^{-1}$ (T60) −287 ppm $°C^{-1}$ (T70)	700 °C	DIW	Chao Wu[99]
Mica	$BaNb_{0.5}Ti_{0.5}O_3$ (BNTO) film	27.5	—	773.15 K	Pulsed laser deposition technology	Cheng Yang[85]
Al_2O_3	ZrB_2/SiCN	4.8	−448 ppm $°C^{-1}$	600 °C	DIW	Fan Lin[100]
Nickel-based alloy (K465)	Pd Cr	1.78 (25 °C) 1.94 (400 °C) 2.03 (600 °C) 2.13 (800 °C)	—	800 °C	Vacuum sputtering deposition technology	Hao Liu[82]
Al_2O_3	ITO	4.1 (1209 °C) 2.1 (1431 °C)	0.0012/°C	1431 °C	RF reactive sputtering	Otto J. Gregory[101]

components necessitates that the strain gauge possess insulating properties. Therefore, when designing *in situ* strain gauges, it is imperative to fabricate an insulating layer on the surface and evaluate its insulating performance at elevated temperatures to ensure the accuracy of strain measurements. The sensitive layer of TFSGs offers a variety of material options, such as ITO, Pt, and TiB_2/SiCN, each exhibiting significantly different properties. The methods employed to prepare these sensitive layers, including magnetron sputtering technology, DIW, pulsed laser deposition technology and so on, also vary considerably. The fabrication method has a profound impact on the performance of the strain gauge. For example, the ITO strain gauge prepared by Li[7,102] using Pulsed Laser Deposition Technology demonstrated a gauge factor of 8.12 at 800 °C, which is higher than that of the ITO strain gauge prepared by Liu[98] using RF Magnetron Sputtering Technology. When preparing strain gauges, it is crucial to consider the requirements of the application scenario, selecting appropriate fabrication methods and sensitive/insulating materials based on the shape of the target substrate. Currently, the highest temperature achieved for strain testing in a laboratory setting is 1431 °C, accomplished by Gregory.[101] However, the resistance of the gauge exhibited a significant decrease within three minutes at this temperature, indicating that there is still a considerable distance to go before it can be applied in engineering contexts.

4.4 Analysis

After analyzing the materials and properties of TFSGs, to provide a comprehensive understanding of material selection for high-temperature strain gauges, we have conducted a comparative analysis of the key materials, fabrication techniques for SAW, optical fiber grating and TFSG sensors. The following Table 4 summarizes these aspects.

Through the comparative analysis of materials and fabrication techniques for high-temperature strain gauges, we can find the distinct advantages and limitations of SAW sensors, optical fiber grating sensors, and thin-film sensors (TFSGs). SAW sensors, typically fabricated from LGS or AlN using photolithography and thin-film deposition, offer high sensitivity but are prone to surface contamination and material degradation at extreme temperatures. In contrast, optical fiber grating sensors, made primarily of silica or ceramic-derived fibers and fabricated through UV laser inscription or fusion splicing, excel in long-term reliability and resistance to electromagnetic interference (EMI), though they face challenges such as material degradation and hydrogen-induced wavelength shifts at very high temperatures. Meanwhile, thin-film sensors (TFSGs) prepared by sputtering and deposition provide excellent strain transfer accuracy and durability but are susceptible to oxidation and thermal cycling effects.

To provide a comprehensive understanding of high-temperature strain gauges, it is essential to discuss their reliability and aging characteristic. These aspects are critical for ensuring their practical deployment and long-term functionality in extreme environments. The long-term reliability and aging characteristics of high-temperature strain gauges are critical for their practical deployment. SAW sensors are prone to aging due to surface contamination and material degradation at high temperatures. However, using robust piezoelectric materials like LGS and protective coatings can significantly improve their lifespan and reliability. FBG sensors, while highly reliable due to the stability of silica fibers, can experience aging effects such as material degradation at extreme temperatures (above 800 °C) and hydrogen-induced wavelength shifts. These issues can be mitigated through advanced packaging and material selection. FPI sensors, particularly those using CDF, exhibit excellent thermal stability and resistance to aging at high temperatures (up to 1000 °C). However, mechanical fatigue in the resonant cavity over prolonged use may affect performance, necessitating regular calibration, which has been confirmed by the experiments conducted by Nicolas L. Schneebeli.[103] TFSG sensors are susceptible to aging due to oxidation and thermal cycling effects at high temperatures. Using high-temperature-resistant materials (*e.g.*, Pt-based alloys) and protective coatings can improve their durability. The methodology for applying sensors to the surface or material being measured is another critical factor. SAW sensors are usually bonded to the surface using high-temperature adhesives or deposited directly onto the substrate using thin-film techniques. Surface preparation, including cleaning and polishing, is essential to ensure optimal performance. FBG and FPI sensors are typically embedded within or surface-mounted on the material. For surface mounting, the material surface must be clean and smooth, and specialized adhesives (*e.g.*, epoxy resins) are used to ensure strong bonding and strain transfer. In high-temperature environments, ceramic-based adhesives are preferred. Huaping Gong[104] investigated the effects of three different adhesives on the performance of FBG strain gauges within the temperature range of 0 to 40 °C, with the following results: FBG sensors fixed with modified acrylate exhibited high linearity, sensitivity, and stability across different temperatures; those fixed with glass glue also demonstrated high linearity and stability but with lower sensitivity; when FBG sensors were fixed with epoxy resin, their sensitivity and linearity were significantly affected by temperature. These findings provide valuable insights for adhesive selection in practical applications. TFSG sensors are typically bonded to the surface using high-temperature cement

Table 4 Comparative analysis of materials and fabrication techniques for high-temperature strain gauges

Sensor type	Key materials	Fabrication techniques
SAW	LGS, quartz, AlN	Photolithography, thin-film deposition
Optical fiber	Silica fiber, Ge-doped fiber	UV laser inscription, fusion splicing
TFSG	Pt, ITO, NiCr, Al_2O_3	Sputtering, thin-film deposition

or sputtered directly onto the substrate. However, for ultra-high-temperature applications (>1200 °C), there are currently no commercially available cements suitable for use. Therefore, it is recommended to employ *in situ* thin-film deposition to form the sensing film directly, eliminating the need for an adhesive layer and improving the accuracy of strain transfer. Surface preparation, including cleaning and roughening, is critical to ensure strong adhesion and accurate strain transfer.

The readout mechanisms of high-temperature strain gauges are critical for ensuring accurate and reliable measurements, with each type of sensor requiring specialized instruments and circuits to convert physical strain into measurable signals. SAW sensors typically rely on radio frequency (RF) signal processing circuits, including RF oscillators, mixers, and frequency counters, to detect changes in surface acoustic waves, often enhanced by advanced techniques like phase-locked loops (PLLs) for improved precision. Optical fiber grating sensors (FBG type and FPI type) commonly use optical interrogators or spectrometers, such as broadband light sources, optical circulators, and high-resolution spectrometers, to measure wavelength shifts in FBG sensors or cavity length changes in FPI sensors, often incorporating photodetectors and signal processing algorithms for higher accuracy. High-temperature TFSGs utilize Wheatstone bridge circuits to convert resistance changes into voltage signals, often integrated with amplifiers and analog-to-digital converters (ADCs) to enhance resolution, while specialized materials and designs ensure the stability of readout electronics under extreme conditions.

5. Applications

Over the past several years, considerable advancements have been achieved in the development of high-temperature strain gauges, particularly in the areas of material innovation, sensor design, and application. New high-temperature materials, such as aluminum-doped zinc oxide (AZO) and carbon-based materials, have garnered attention for their excellent thermal stability and sensitivity.[105] Concurrently, the structural design of these sensors is being optimized to enhance sensitivity and improve resistance to interference. Furthermore, high-temperature strain gauges are being miniaturized and integrated using technologies such as MEMS, facilitating their installation in confined spaces.

High-temperature strain gauges are primarily utilized to measure the strain changes in materials under extreme temperature conditions. The sensors exhibit a broad spectrum of utility across aerospace, energy, and industrial surveillance domains. They typically employ specific technologies to ensure stable and accurate operation in high-temperature environments. Such sensors are deployed in aero-engines, vehicle structures, rockets, and spacecraft to monitor thermal stress and material strain. For instance, the FBG strain gauge has been extensively used for high-temperature measurements in oil wells due to their advantages, including high-temperature resistance, electromagnetic interference resistance, and multi-parameter measurement capabilities (Fig. 7a).[106] Furthermore, FBG sensors are also suitable for conducting high-temperature

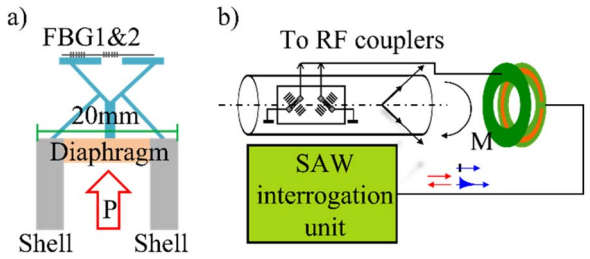

Fig. 7 Application of high-temperature strain gauge: (a) schematic diagram of the application of an optical fiber grating high-temperature strain gauge in oil Wells;[82] (b) SAW high-temperature strain gauge in the application diagram in the automotive industry.[83]

measurements within oil well environments. The FBG cavity of its sapphire fiber can withstand temperature limits exceeding 1000 °C while maintaining stable and accurate measurement capabilities in extreme environments,[107] thereby providing reliable data support in complex application scenarios. In the automotive industry, a SAW high-temperature strain gauge is deployed for the surveillance of stress levels in critical components including engines, exhaust assemblies, and underbodies (refer to Fig. 7b).

These sensors are designed to function effectively under extreme thermal conditions, providing instantaneous data that is instrumental in improving vehicular safety and operational efficiency.[108]

Under extreme high-temperature conditions, high-temperature strain gauges are extensively utilized to quantify the stress and strain of aerospace engines, thereby guaranteeing their dependable operation within the confines of ultra-high-temperature environments. In the case of fiber optic strain gauges, strain measurements at elevated temperatures are typically accomplished by welding both extremities to the engine casing or turbine blades. As an illustrative example, Ping Xia[44] and colleagues secured the ends of the optical fiber to a metal plate *via* metal sheet welding, and they employed

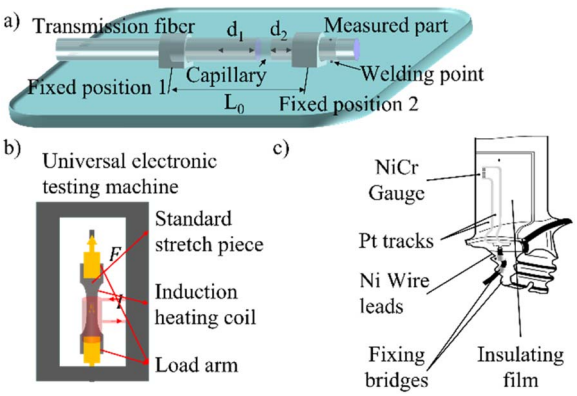

Fig. 8 Strain gauges for aerospace applications: (a) conceptual diagram illustrating the installation of a FBG strain gauge on a metallic shell;[38] (b) inductive heating-type universal testing machine incorporating standard tensile specimens; (c) schematic representation of the fabrication of a NiCr TFSG on a turbine blade.[85]

a muffle furnace to generate a high-temperature environment, successfully measuring the stress and strain of the metal plate under such conditions. This method offers insights into the assessment of stress and strain within the aircraft engine housing during operational phases. The schematic representation can be found in Fig. 8a.

For TFSGs, to facilitate a closer approximation to actual application scenarios, the substrate is typically fabricated from high-temperature-resistant materials commonly employed in the casting of aerospace engines, including the Ni-based superalloy GH3536,[49] which is designed as a standard stretching part. The high-temperature environment is supplied either by an induction coil or a high-temperature furnace. Tensile calibration is performed using a universal testing machine to ensure that the calibration environment is more aligned with the actual testing conditions. The schematic diagram is presented in Fig. 8b.

Furthermore, NASA has developed sophisticated high-temperature strain gauges tailored for hypersonic vehicles to assess the safety and viability of novel materials and structural designs. Kayser[109] fabricated a NiCr film strain gauge deposited on the TM-333 engine blade. The study revealed that the relative resistance variation at 700 °C was 0.3%/h, and short-term dynamic strain measurements were feasible at 800 °C, with demonstrated oxidation resistance, high-temperature stability, and repeatability. This technology finds applications in turbine engine technology, as depicted in Fig. 8c.

Lei[110] investigated a PdCr TFSG on the surface of ceramic turbine blades. The strain gauge exhibited a stable linear relationship with the loading force at 1050 °C, with the strain factor decreasing by only approximately 22% from room temperature to 1050 °C. The PdCr strain gauges produced by Lei were structurally similar to those by Kayser[109], both featuring the patterning of sensitive materials on turbine blades, thereby providing a technical reserve for the measurement of stress and strain distributions during turbine blade operation.

These sensors are widely employed across various applications, and their performance is anticipated to undergo significant enhancement alongside the progression of scientific and technological advancements.

6. Future directions

The high-temperature strain gauge is a promising device due to its advantages, including high temperature tolerance, stability, and sensitivity. Currently, high-temperature strain gauges serve as essential measurement tools, playing a significant role in numerous demanding applications. With the progression of sensor technology, there is a concentrated effort among researchers to innovate and fabricate novel high-temperature-resistant materials, including sophisticated ceramics and superalloys, with the aim of improving the operational efficiency and robustness of these sensors. Concurrently, high-temperature strain gauges are evolving towards greater integration and intelligence, resulting in smaller sizes and the incorporation of additional functions, thereby enhancing their applicability in complex environments. The multi-functional and multi-channel data acquisition systems can simultaneously measure various parameters, including strain and temperature, which improves the overall performance and convenience of the system. Furthermore, the use of intelligent data acquisition instruments increases the efficiency and accuracy of data processing.

In the future, it is highly probable that high-temperature strain gauges will evolve along several key trajectories:

Material innovation: high-temperature strain gauges employing polymer precursor SiCN ceramics exhibit corrosion resistance,[111] high sensitivity, and ultra-fast response rates, which encompasses a measurement spectrum from ambient temperature to 1000 °C. MXene, as an emerging material, exhibits exceptional electronic, mechanical, electrochemical, and optical properties.[112] Current research on this material primarily focuses on its performance within room to moderate temperature ranges (typically below 600 °C). For instance, monolayer MXene demonstrates outstanding thermal stability in air up to 600 °C, while multilayer MXene can achieve comparable stability through vacuum annealing at 600 °C.[113] For ultra-high-temperature applications, integration with other materials may enhance thermal stability. As demonstrated by Kai Wang *et al.*,[114] a sensor fabricated by integrating MXene with a vermiculite/sodium alginate composite exhibited merely ~5 Ω resistance variation after exposure to 1300 °C for 60 seconds, suggesting MXene's potential as a high-temperature strain material. Regarding ceramic-based large-range strain gauges, microcracks may develop during tensile loading, causing dramatic resistance changes and eventual sensor failure. Self-healing ceramics could theoretically address this issue through oxidation-induced healing or precipitation-induced healing mechanisms,[115] which would maintain minimal resistance variation pre- and post-repair. However, no literature reporting such electrical stability during the healing process has been identified to date. The incorporation of innovative materials constitutes a pivotal pathway for the advancement of high-temperature strain sensing technology in the future.

Flexible miniaturization design: a novel high-temperature multi-parameter sensor has been successfully developed through a thermal resistance thin film array structure and highly reliable preparation technology for composite flexible thin films.[116] These sensors demonstrate exceptional performance in high-temperature environments, marking a breakthrough in flexible miniaturization design within the field of high-temperature strain gauges.

Extreme environment measurement capability: Professor Li Yibin's team at Beihang University successfully measured the strain field in an ultra-high temperature environment of 3000 °C using their self-developed UV-digital image correlation (UV-DIC) system.[117] This achievement highlights the potential of high-temperature strain gauges in extreme environments.

Application of MEMS technology: the advancement of MEMS high-temperature silicon pressure sensors necessitates breakthroughs in key technologies such as low-stress leadless packaging, temperature compensation, and high-temperature special circuit (ASIC) chips. These technological advancements

will facilitate the mass production of high-precision and high-reliability high-temperature strain gauges.

Characterized by attributes including elevated sensitivity, robust high-temperature tolerance, electromagnetic interference insensitivity, and corrosion resilience, these sensors have found widespread application in many critical fields. As technology continues to progress, these sensors are expected to achieve further breakthroughs in intelligence, multi-parameter integration, and miniaturization, thereby promoting their application and development across various domains.

7. Conclusion

Strain gauges designed for high-temperature conditions are indispensable instruments for quantifying the deformation and stress experienced by materials or structural components within extreme thermal environments. This article provides an in-depth exploration of the working principles, types, material selection, and applications of the three major categories of high-temperature strain gauges: SAW strain gauge, optical fiber grating strain gauge (FBG and FPI), and TFSG. Each type of the three gauges has its unique advantages and limitations. SAW sensors offer high sensitivity and fast response times but are prone to surface contamination and material degradation at extreme temperatures. Optical fiber grating sensors, particularly FBG and FPI, excel in long-term reliability and resistance to electromagnetic interference, yet their performance can be affected by material degradation and hydrogen-induced wavelength shifts at very high temperatures. High-temperature TFSG provide excellent strain transfer accuracy and durability but face challenges related to oxidation and thermal cycling effects.

As key monitoring instruments, these sensors offer precise strain measurements under extreme conditions, thereby effectively ensuring the safety of structures and equipment. By comparing the different types of high-temperature strain gauges, we emphasize the importance of selecting the appropriate sensor type and material to guarantee stability and durability under high-temperature conditions. Furthermore, this paper discusses future development trends, such as the integration of miniaturization, intelligence, and data analysis. The application prospects of high-temperature strain gauges in fields like aerospace and industrial monitoring are extensive, provided that ongoing research addresses their limitations and enhances their performance in extreme environments.

Data availability

Data availability is not applicable to this article as no new data were created or analyzed in this study.

Author contributions

Xiang Liu assisted in literature writing and image drawing; Zhongkai Zhang provided the idea; Jiaxing Wang and Meng Wang assisted in some literature writing; Tao Lin, Yantao Liu and Qing Tan Assisted in investigating the literature; Rui Qi helped in formal analysis; Zhaojun Liu assisted in review and editing; Bian Tian provided research guidance and supervision.

Conflicts of interest

There are no conflicts to declare.

Acknowledgements

This work is supported by The National Key Research and Development Program of China (No. 2022YFB3206400), the National Natural Science Foundation of China (No. 52475570), the S&T Program of Energy Shaanxi Laboratory (No. ESLB202437), the Key Research and Development Program of Shaanxi (No. 2025CY-YBXM-053) and the Key Laboratory for Precision/Non-traditional Machining and Micromanufacturing Technology of Ministry of Education, Dalian University of Technology (B202503).

References

1 L. Pu, H. J. Ma, J. C. Dong, C. Zhang, F. L. Lai, G. J. He, P. M. Ma, W. F. Dong, Y. P. Huang and T. X. Liu, *Nano Lett.*, 2022, **22**, 4560–4568.
2 J. C. Dong, Y. D. Peng, J. Y. Long, Y. X. Zhang, Z. C. Wang, T. E. Park, Y. P. Huang and T. X. Liu, *Adv. Funct. Mater.*, 2023, **33**, 41.
3 J. C. Dong, X. W. Tang, Y. D. Peng, C. H. Fan, L. Li, C. Zhang, F. L. Lai, G. J. He, P. M. Ma, Z. C. Wang, Q. F. Wei, X. P. Yan, H. L. Qian, Y. P. Huang and T. X. Liu, *Nano Energy*, 2023, **108**, 108194.
4 L. Pu, Y. P. Liu, L. Li, C. Zhang, P. M. Ma, W. F. Dong, Y. P. Huang and T. X. Liu, *ACS Appl. Mater. Interfaces*, 2021, **13**, 47134–47146.
5 J. C. Dong, D. Wang, Y. D. Peng, C. Zhang, F. L. Lai, G. J. He, P. M. Ma, W. F. Dong, Y. P. Huang, I. P. Parkin and T. X. Liu, *Nano Energy*, 2022, **97**, 107160.
6 G. Peixin, Y. Tao, Y. Zhang, W. Jiao and Z. Jingyu, *Chin. J. Aeronaut.*, 2021, **34**, 83–114.
7 S. Li, L. Zhang, H. Xie, X. Yao, Z. Hao, H. Dong and Q. Tan, *IEEE Sens. J.*, 2023, **23**, 11490–11497.
8 D. Klaas, R. Ottermann, F. Dencker and M. C. Wurz, *Sensors*, 2020, **20**, 3294.
9 X. Li, Q. Tan, L. Qin, X. Yan and X. Liang, *Micromachines*, 2022, **13**, 912.
10 W. Wang, X. Liu, S. Mei and Y. Jia, *Sensor. Actuator.*, 2019, **287**, 157–164.
11 M. Li, H. Kan and S. Che, *et.al.*, *Sensor. Actuator.*, 2019, **287**, 241–249.
12 L. Zhang, Y. Liu, X. Gao and Z. Xia, *Appl. Opt.*, 2015, **54**, E109–E112.
13 Y. Zhao, Y. Liu, Y. Li and Q. Hao, *Sensors*, 2020, **20**, 5826.
14 C. Wu, Y. Fu, Y. Zeng, G. Chen, X. Pan, F. Lin, L. Xu, Q. Chen, D. Sun and Z. Hai, *Chem. Eng. J.*, 2023, **463**, 142518.
15 D. Mandal and S. Banerjee, *Sensors*, 2022, **22**, 3.

16 F. Li, T. Shen, C. Wang, Y. Zhang, J. Qi and H. Zhang, *Nano-Micro Lett.*, 2020, **12**, 1–44.
17 T. X. Ma and C. Fu, *Crystals*, 2024, 997.
18 J. Zhou, Y. Guo, Y. Wang, Z. Ji, Q. Zhang, F. Zhuo, J. Luo, R. Tao, J. Xie and J. Reboud, *Appl. Phys. Rev.*, 2023, **10**, 2.
19 J. Curie and P. Curie, *Bull. Mineral.*, 1880, **3**, 90–93.
20 S. B. A. Rani, *Current Applied Physics*, Elsevier, 2024.
21 Y. Meng, G. Chen and M. Huang, *Nanomaterials*, 2022, **12**, 7.
22 D. Yi, F. Liu and Y. Geng, *Opt. Express*, 2021, **29**(12), 18624–18633.
23 C. E. Campanella, A. Cuccovillo, C. Campanella, A. Yurt and V. M. Passaro, *Sensors*, 2018, **18**, 3115.
24 M. Bonopera, *Materials*, 2022, **15**, 5561.
25 X. Qian, L. Xu, L. Su, L. Tang, S. Ouyang, X. Zhou, M. Wu, C. Wu and L. Wang, *Surf. Interfaces*, 2024, **55**, 105324.
26 Y. Liu, H. Jiang, X. Zhao, X. Deng and W. Zhang, *Appl. Surf. Sci.*, 2022, **579**, 152169.
27 G. He, Y. He, L. Xu, L. Li, L. Wang, Z. Hai and D. Sun, *Micromachines*, 2023, **14**, 1719.
28 A. Aabid, M. A. Raheman, Y. E. Ibrahim, A. Anjum, M. Hrairi, B. Parveez, N. Parveen and J. Mohammed Zayan, *Sensors*, 2021, **21**, 4145.
29 R. W. Schwartz, J. Ballato and G. H. Haertling, in *Ceramic Materials for Electronics*, CRC Press, 2018, pp. 223–244.
30 C. Zhe, Z. Jian, T. Hao, L. Yi, S. Yiping, Y. Xiaobo, Z. Jiangpo, Z. Hongshuai, W. Jiangning, S. Xianglong, C. Yiqin, F. Yong Qing and D. Huigao, *ACS Sens.*, 2020, 1657–1664, DOI: **10.1021/acssensors.0c00259**.
31 Z. Xuhang, T. Qiulin, L. Xiaorui, L. Baimao, G. Tao and G. Yu, *Micromachines*, 2021, 643, DOI: **10.3390/mi12060643**.
32 Z. Yang, F. Wang, W. Nie, X. Han, X. Guo, X. Shan, X. Lin, H. Dun, Z. Sun, Y. Xie and K. Zhang, *Sens. Actuators, A*, 2023, **357**, 114379.
33 Z. Daiqing, Z. Yihong, X. Weipeng, C. Jinkai, Z. Miling, Z. Jikai, J. Hao, D. Shurong and L. Jikui, *J. Alloys Compd.*, 2023, 169056, DOI: **10.1016/j.jallcom.2023.169056**.
34 A. Fernández-García, V. I. Solís-Tinoco and M. A. A. Arce, *Int. J. Numer. Model.: Electron. Netw. Devices Fields*, 2023, **37**, 5.
35 L. Xueling, W. Wen, F. Shuyao, Y. Yining, L. Yong and L. Mengwei, *Sensors*, 2020, 2441, DOI: **10.3390/s20092441**.
36 Y. Ruan, Y. Chen, Y. Wu, M. Shi, Y. Du, Z. Song, Y. Chen, H. Dong, C. Zhang and J. Teng, *Chemosensors*, 2023, **11**, 225.
37 L. Juan, L. Chaowei, Y. Hua, Y. Zhen, L. Bin, H. Xingdao and W. Qiang, *Photonic Sens.*, 2020, 341–349, DOI: **10.1007/s13320-020-0596-z**.
38 L. Aiwu, S. Tian-qi, G. Qi, P. Xuepeng, L. Shanren, C. Chao and Y. Yong-Sen, *Chin. Opt.*, 2022, 609–624, DOI: **10.37188/co.2021-0219**.
39 Z. Wujun, W. Xuqiang, Z. Cheng, G. Lei, S. Jinhui, Z. Xiaonan, M. Shengquan, L. Jiaran and Y. Benli, *Opt. Commun.*, 2022, 127543, DOI: **10.1016/j.optcom.2021.127543**.
40 Z. Wang, H. Liu, Z. Ma, Z. Chen, T. Wang and F. Pang, *Opt. Express*, 2019, **27**, 27691.
41 Z. Li, W. Dang, J. Dan, K. Jin, P. Nan, G. Xin, K.-S. Lim, H. Ahmad and H. Yang, *Opt. Fiber Technol.*, 2023, **79**, 103361.
42 S. Lin, Y. Qu, H. Zhang, F. Wang, X. Han and Y. Zhang, *IEEE Sens. J.*, 2023, **23**, 19351–19358.
43 y. Yu, L. Ma, R. Huang, D. Liang, Y. Zhang, C. Du, S. Ruan, S. Fu, J. Zhang and J. Yang, *Presented in Part at the AOPC 2019: Optical Fiber Sensors and Communication*, 2019.
44 P. Xia, Y. Tan, C. Yang, Z. Zhou and K. Yun, *Sensors*, 2021, **21**, 4989.
45 Z. Zhao, W. Ni, C. Yang, S. Ran and P. P. Shum, *IEEE Sens. J.*, 2023, **23**, 24575–24582.
46 R. Shi, H. Chen, X. Fan, C. Liu, H. Li, Z. Gao, S. Zhang, M. Gu, L. Li and Y. Zheng, *IEEE Trans. Instrum. Meas.*, 2024, **73**, 1–10.
47 J. D. Wrbanek and G. C. Fralick, *Thin Film Physical Sensors for High Temperature Applications*, 2020, **https://ntrs.nasa.gov/citations/20205008638**.
48 L. Hao, J. Shuwen, Z. Xiaohui, J. Hongchuan and Z. Wanli, *Sens. Actuators, A*, 2018, 272–277, DOI: **10.1016/j.sna.2018.06.032**.
49 H. Liu, X. Mao and S. Jiang, *Sens. Actuators, A*, 2021, **331**, 113033.
50 L. Hao, M. Xiling, C. Jinting, J. Shuwen and Z. Wanli, *Ceram. Int.*, 2019, 24343–24347, DOI: **10.1016/j.ceramint.2019.08.151**.
51 T. Zhang, L. Yang, J. Ruan, C. Zhang and Q. Chi, *Macromol. Mater. Eng.*, 2021, **306**, 2100514.
52 J. Zhang, H. Jin, J. Chen, W. Xuan, R. Ding, S. Dong and J. Luo, *Sens. Actuators, A*, 2022, **338**, 113464.
53 X. Shi, D. Shi and H. Yang, *Appl. Phys.*, 2020, **10**(3), 198–204.
54 C. Zhao, W. Geng, X. Qiao, F. Xue, J. He, G. Xue, Y. Liu, H. Wei, K. Bi and Y. Li, *Sens. Actuators, A*, 2022, **333**, 113230.
55 J. Zhang, D. Mu, Z. Zhang, H. Jin, J. Chen, W. Xuan, S. Dong and J. Luo, *J. Phys.: Conf. Ser.*, 2024, **2822**, 012117.
56 F. B. Hu, L. N. Cheng, S. Y. Fan, X. F. Xue, Y. Liang, M. H. Lu and W. Wang, *Sens. Actuators, A*, 2022, **333**, 113298.
57 A. Maskay and M. P. da Cunha, *Sens. Actuators, A*, 2017, **259**, 34–43.
58 W. Wang, X. F. Xue, S. Y. Fan, M. W. Liu, Y. Liang and M. H. Lu, *Sens. Actuators, A*, 2020, **308**, 112015.
59 L. Shu, X. M. Wang, L. Li, D. W. Yan, L. P. Peng, L. Fan and W. D. Wu, *Sens. Actuators, A*, 2019, **293**, 14–20.
60 L. Shu, B. Peng, Z. B. Yang, R. Wang, S. Y. Deng and X. Z. Liu, *Sensors*, 2015, **15**, 28531–28542.
61 S. Fan, W. Wang, X. Li, Y. Jia, Y. Sun and M. Liu, *Sensors*, 2020, **20**, 4160.
62 F. Hu, L. Cheng, S. Fan, Y. Liang, M. Liu and W. Wang, *Sens. Actuators, A*, 2021, DOI: **10.1016/j.sna.2021.113298**.
63 W. Min, L. Yan, Q. Yuanhang, G. Xiyu, W. Yilin, L. Wenjuan, C. Yao, G. Shishang and S. Chengliang, *Electronics*, 2023, 3863, DOI: **10.3390/electronics12183863**.
64 J. Streque, J. Camus, T. Laroche, S. Hage-Ali, H. M'Jahed, M. Rammal, T. Aubert, M. A. Djouadi, S. Ballandras and O. Elmazria, *IEEE Sens. J.*, 2020, **20**, 6985–6991.
65 T. Xue, F. Xu, Q. Tan, X. Yan and X. Liang, *Sens. Actuators, A*, 2022, **334**, 113315.

66 L. Kelly, C. Chen, X. Bao and P. Berini, *Sens. Actuators, A*, 2022, **338**, 113504.
67 T. Li, Y. Bu, Y. Zheng, N. Wang and Y. Tan, *Mech. Syst. Signal Process.*, 2023, **200**, 110605.
68 L. Jincheng, Z. Qi, S. Yang, T. Jiacheng, T. Jianhua, P. Fei and X. Hai, *Opt. Laser Technol.*, 2020, 106223, DOI: 10.1016/j.optlastec.2020.106223.
69 L. Chen, Y. Feng, P. Liu and K. Ding, *Research on Static Fatigue Failure and Life Prediction of High Temperature Resistant Fiber Bragg Grating Sensors*, 2024, DOI: 10.1109/ECIE61885.2024.10626616.
70 J. He, H. Li, X. Xu, J. He, C. Liao, Y. Wang and Y. Yang, *Presented in Part at the Thirteenth International Conference on Information Optics and Photonics (CIOP 2022)*, 2022.
71 C. Tan, Z. Dong, Y. Li, H. Zhao, X. Huang, Z. Zhou, J.-W. Jiang, Y.-Z. Long, P. Jiang, T.-Y. Zhang and B. Sun, *Nat. Commun.*, 2020, **11**, 3530.
72 J. S. Li, P. G. Jia, J. Qian, J. Wang, G. W. An and J. J. Xiong, *Appl. Opt.*, 2022, **61**, 3743–3747.
73 T. Y. He, M. Q. Chen, Y. Zhao and H. M. Wei, *Opt. Laser Technol.*, 2022, **152**, 108106.
74 C. Ghosh and V. Priye, *IEEE Sens. J.*, 2020, **20**, 14181–14186.
75 C. Wang, Y. M. Zhang, Q. S. Huang, Z. W. Luo and Y. Gao, *Appl. Opt.*, 2025, **64**, 1731–1737.
76 Y. J. Jiang, D. X. Yang, Y. Yuan, J. Xu, D. Li and J. L. Zhao, *Appl. Opt.*, 2016, **55**, 6341–6345.
77 X. Liu, P. Y. Nan, J. J. Zhu, Z. R. Li, J. X. Dan, W. J. Dang, K. S. Lim, W. Udos, H. Ahmad, X. C. Liu and H. Z. Yang, *Opt. Commun.*, 2022, **508**, 127717.
78 J. Nan, D. S. Zhang, X. Y. Wen, M. Li, H. F. Lv and K. Su, *IEEE Sens. J.*, 2020, **20**, 5270–5276.
79 Q. Tian, G. G. Xin, K. S. Lim, Y. D. He, J. Liu, H. Ahmad, X. C. Liu and H. Z. Yang, *Opt. Express*, 2020, **28**, 30478–30488.
80 Z. Lv, C. Zhang, Y. Wang, Z. Kang, X. Gao and Y. Guo, *Thin Solid Films*, 2023, **773**, 139780.
81 L. C. Martin and R. Holanda, *Applications of Thin Film Thermocouples for Surface Temperature Measurement*, 1994.
82 H. Liu, X. Mao, Z. Yang, J. Cui, S. Jiang and W. Zhang, *Sens. Actuators, A*, 2019, **298**, 111571.
83 S. Yang, C. Zhang, X. Chang, J. Huang, Z. Yang, J. Yao, H. Wang and G. Ding, *Ceram. Int.*, 2019, **45**, 17048–17053.
84 Z. Liu, J. Liang, H. Zhou, W. Lu, J. Li, B. Wang, Q. Li, X. Zhao and J. Xu, *Appl. Surf. Sci.*, 2022, **594**, 153508.
85 C. Yang, M. Guo, D. Gao, W. He, J. Feng, A. Zhang, Z. Fan, D. Chen, M. Zeng, S. Wu, J. Gao, C. F. Guo, G. Zhou, X. Lu and J. Liu, *Adv. Mater. Technol.*, 2019, **4**, 1900578.
86 M. Guo, C. Yang, D. Gao, Q. Li, A. Zhang, J. Feng, H. Yang, R. Tao, Z. Fan, M. Zeng, G. Zhou, X. Lu and J. M. Liu, *J. Mater. Sci. Technol.*, 2020, **44**, 42–47.
87 Y. Li, P. Zhou, Y. Qi and T. Zhang, *J. Am. Ceram. Soc.*, 2021, **105**, 2038–2045.
88 C. Wu, F. Lin, Y. Fu, Y. Zeng, G. Chen, L. Xu, X. Pan, Q. Chen, D. Sun and Z. Hai, *Surf. Coat. Technol.*, 2023, **459**, 129380.
89 Y. Zhao, Y. Li, Y. Wu, G. Ding and C. Zhang, *IEEE Sens. J.*, 2024, 9573–9584.
90 Y. Cui, X. Li, T. Zhang, W. Ding and J. Yin, *Sensors*, 2022, **22**, 7595.
91 T. S. F Li, C. Wang, Y. Zhang, J. Qi and H. Zhang, *Nano-Micro Lett.*, 2020, 173.
92 K. Singh, S. Sharma, S. Shriwastava, P. Singla, M. Gupta and C. Tripathi, *Mater. Sci. Semicond. Process.*, 2021, **123**, 105581.
93 C. Wu, F. Lin, X. C. Pan, Y. J. Zeng, G. C. Chen, L. D. Xu, Y. P. He, G. H. He, Q. N. Chen, D. H. Sun and Z. Y. Hai, *Chem. Eng. J.*, 2023, **457**, 141269.
94 C. Tang, S. Zeng, H. Hong, Y. Fang, Y. Li, Y. Wang, M. Zhu, J. Sun and T. Deng, *Surf. Interfaces*, 2023, **40**, 103029.
95 X. Pan, F. Lin, C. Wu, Y. Zeng, G. Chen, Q. Chen, D. Sun and Z. Hai, *Micromachines*, 2022, **13**, 1472.
96 C. Wu, Y. He, L. Li, G. Chen, Y. Fu, Y. Zeng, L. Xu, F. Lin, X. Pan, Q. Chen, Y. Zhao, D. Sun and Z. Hai, *Adv. Eng. Mater.*, 2023, **25**, 2300516.
97 C. Wu, F. Lin, X. Pan, Y. Zeng, Y. Fu, G. Chen, Y. He, Q. Chen, D. Sun and Z. Hai, *IEEE Sens. J.*, 2022, **22**, 22473–22478.
98 Z. Liu, J. Liang, H. Zhou, H. Sun, W. Lu, B. Wang, Q. Li, X. Zhao, D. Wang and J. Xu, *Appl. Surf. Sci.*, 2023, **608**, 155292.
99 C. Wu, X. Pan, F. Lin, Z. Cui, Y. He, G. Chen, Y. Zeng, X. Liu, Q. Chen, D. Sun and Z. Hai, *IEEE Sens. J.*, 2022, **22**, 11517–11525.
100 F. Lin, X. Pan, C. Wu, Y. Zeng, G. Chen, Q. Chen, D. Sun and Z. Hai, *Micromachines*, 2022, **13**, 1472.
101 O. J. Gregory, T. You and E. E. Crisman, *Thin Solid Films*, 2005, **476**, 344–351.
102 S. L. Li, L. Zhang, H. Xie, X. Yao, Z. Y. Hao, H. L. Dong and Q. L. Tan, *IEEE Sens. J.*, 2023, **23**, 11490–11497.
103 N. L. Schneebeli, I. V. Cavalcante, E. M. Morais, M. J. Pontes, C. Marques and A. J. R. Leal, *IEEE Sens. J.*, 2023, **23**, 30378–30385.
104 H. P. Gong, X. R. Li, Y. X. Jin and X. Y. Dong, *Adv. Mater. Res.*, 2011, **301–303**, 415–420.
105 Q. Zhou, D. Yang, P. Xu, W. Xue and N. Liao, *Chem. Eng. J.*, 2024, **484**, 149758.
106 D. Xu, D. Feng, Q. Chen, G. Liu and X. Qiao, *Sens. Actuators, A*, 2023, **357**, 114397.
107 S. Ma, Y. Xu, Y. Pang, X. Zhao, Y. Li, Z. Qin, Z. Liu, P. Lu and X. Bao, *Sensors*, 2022, **22**, 5722.
108 V. Kalinin, *Wireless Physical SAW Sensors for Automotive Applications*, 2011, pp. 212–221.
109 P. Kayser, J. C. Godefroy and L. Leca, *Sens. Actuators, A*, 1993, **37–8**, 328–332.
110 J.-F. Lei, L. C. Martin and H. A. Will, *Advances in Thin Film Sensor Technologies for Engine Applications*, American Society of Mechanical Engineers, 1997.
111 M. Yang, C. Ma, Y. Hu, K. Wang, R. Zhao, Y. Liang, D. Han, H. Wang, R. Zhang and G. Shao, *Adv. Funct. Mater.*, 2024, 2400400.
112 M. Naguib, M. Kurtoglu, V. Presser, J. Lu, J. J. Niu, M. Heon, L. Hultman, Y. Gogotsi and M. W. Barsoum, *Adv. Mater.*, 2011, **23**, 4248–4253.

113 H. Fang, A. Thakur, A. Zahmatkeshsaredorahi, Z. Y. Fang, V. Rad, A. A. Shamsabadi, C. Pereyra, M. Soroush, A. M. Rappe, X. G. Xu, B. Anasori and Z. Fakhraai, *Proc. Natl. Acad. Sci. U. S. A.*, 2024, **121**, e2400084121.
114 K. Wang, Y. F. Wang, A. R. Yao, H. Y. Hu, W. H. Fan, S. J. Lin and J. W. Lan, *Chem. Eng. J.*, 2025, **505**, 159483.
115 S. Aouadi, J. Gu and D. Berman, *J. Vac. Sci. Technol., A*, 2020, **38**, 5.
116 J. Liu, L. Xu, X. Zhou, F. Zhao, Y. Wang, S. Wang, W. Lv, D. Sun and Q. Chen, *Coatings*, 2024, **14**, 967.
117 Y. Luo and Y. Dong, *NDT E Int.*, 2024, 103155.